Biogeosciences, 23, 1965–1985, 2026
https://doi.org/10.5194/bg-23-1965-2026

Biogeosciences Open Access EGU

Photochemistry of the sea-surface microlayer (SML) influenced by a phytoplankton bloom: a mesocosm study

Olenka Jibaja Valderrama, Daniele Scheres Firak, Thomas Schaefer, Manuela van Pinxteren, Khanneh Wadinga Fomba, and Hartmut Herrmann

Atmospheric Chemistry Department (ACD), Leibniz-Institute for Tropospheric Research (TROPOS), Leipzig, 04318, Germany

Correspondence: Hartmut Herrmann (herrmann@tropos.de)

Received: 21 August 2025 – Discussion started: 29 August 2025
Revised: 2 February 2026 – Accepted: 9 February 2026 – Published: 16 March 2026

Abstract. The sea-surface microlayer (SML) is the thin boundary interface between the ocean and the atmosphere, and it is expected to play a crucial role in atmospheric chemistry on a global scale. Being a biologically-enriched environment exposed to strong actinic radiation, the SML is potentially a hotspot for photochemical reactions that have relevance in the transformation and cycling of organic compounds. The present study explores the photochemical production and degradation of carbonyl compounds, as well as the photochemical oxidation capacity in both ambient SML and underlying water (ULW) samples. Natural seawater samples were collected during a mesocosm study where a phytoplankton bloom was induced through the controlled addition of inorganic nutrients. To assess the photochemistry of carbonyl compounds, collected SML and ULW samples were irradiated for 5 h. The photochemical formation and degradation of 17 carbonyl compounds were quantified by monitoring compound-specific changes in concentrations, which varied significantly across the samples. Before irradiation, values in the SML ranged from 201–762 nmol L^{-1} in the pre-bloom phase, 984–4591 nmol L^{-1} in the bloom phase, and 647–4894 nmol L^{-1} in the post-bloom phase; while in the ULW they were significantly lower (e.g., 136–366 nmol L^{-1} in the bloom phase). After 5 h of irradiation, the concentrations of carbonyl compounds increased further, reaching up to 6026 nmol L^{-1} in the SML during the bloom phase and 419 nmol L^{-1} in the ULW. Experimental evidence suggests an enhanced photochemical activity in the SML during the bloom phase for glyoxal, methylglyoxal, methyl vinyl ketone (MVK), methacrolein, acrolein, crotonaldehyde, heptanal, biacetyl, hexanal and trans-2-hexenal. The observed photooxidation capacity of the seawater samples indicate a dominant influence of redox active species like metal ions, rather than of the phytoplankton bloom phases. The overall photochemical oxidation capacity was similar for both SML and ULW samples, with average values of 34 µM s^{-1}. Our findings show an influence of biological activity in the photochemistry of carbonyl compounds in the SML and its implications for the emission of volatile organic compounds (VOCs) to the marine atmosphere, pointing to the complex interaction of biotic and abiotic factors in the air–sea boundary and underscoring the relevance of marine photochemistry in biogeochemical processes.

1 Introduction

The sea-surface microlayer (SML) is the uppermost boundary layer of the ocean. With a thickness typically between 1 and 1000 µm, the SML potentially covers up to 70 % of the Earth's surface (Wurl et al., 2017, 2011, 2016; Hardy, 1982). This specific environment is characterized by its enrichment in dissolved organic matter (DOM), particulate organic matter (POM) and inorganic matter, and its direct exposure to solar radiation, both factors presumably leading to photochemical transformations that result in a diverse mixture of chemical compounds (Hardy, 1982; Zafiriou, 1977). The SML naturally acts as an interface between the underlying water (ULW) and the atmosphere, and many transfer processes, such as those involving particles or trace gases, are mediated through the SML and its respective properties (Engel et al., 2017; Wurl et al., 2017). Clearly, based on its

biological, chemical and physical properties, the SML can be distinguished from ULW.

The DOM present in the SML includes carbohydrates, lipids, amino acids, proteins and humic substances, which are primarily produced by marine biota during phytoplankton growth, grazing and viral lysis (Lampert, 1978; Lancelot, 1979; Hansell and Carlson, 2002; Liss et al., 1997; Carpenter and Nightingale, 2015). A portion of the total DOM, the coloured dissolved organic matter (CDOM), absorbs light in the ultraviolet and visible region, leading to photochemical transformation and production of reactive species (Coble, 2007; Rochelle-Newall et al., 1999). The SML also has light-absorbing molecules that transfer energy to other compounds and trigger photochemical transformations, known as photosensitizers (Mopper and Stahovec, 1986; Momzikoff et al., 1983). Photosensitizers do not only enhance photochemical reactions in seawater, but their decay releases fragments of photosynthetic structures rich in pigments that may also undergo photochemical degradation (Zafiriou, 1977).

Under exposure to sunlight, CDOM and humic substances in seawater undergo photochemical reactions that form species like carbonyl compounds. Field-based measurements provided evidence of oceanic production of aldehydes like formaldehyde, acetaldehyde, glyoxal, methylglyoxal, propanal, and hexanal; and ketones like acetone (de Bruyn et al., 2011; Kieber et al., 1990; Mopper and Stahovec, 1986; Mopper et al., 1991; van Pinxteren and Herrmann, 2013; Zhu and Kieber, 2019, 2018). However, there are still considerable doubts regarding the rates in which these processes occur and their interplay with biological events. Furthermore, investigations on the photochemistry in seawater of additional carbonyl compounds with potential relevance in the marine environment are, to this moment, still limited.

Carbonyl compounds serve as energy sources for marine microorganisms (de Bruyn et al., 2017; Dixon et al., 2014). Due to their high volatility, carbonyl compounds produced in the SML are also potential precursors of oxygenated volatile organic compounds (OVOCs) in the marine atmosphere. OVOCs can contribute to the formation of free radicals and secondary organic aerosols (SOAs), therefore impacting air quality, the atmospheric oxidative capacity and cloud formation.

Photochemistry in the SML plays a critical role in global biogeochemistry by influencing marine carbon cycling and atmospheric chemistry in the marine environment (Tinel et al., 2023). Both the fate of DOM and the formation of volatile organic compounds (VOCs) in seawater are highly impacted by its photochemical oxidation capacity, governed by the sunlight-driven production of excited triplet-state CDOM (^{3}CDOM*) and reactive oxidants. These processes occur alongside or even exceed biological pathways of transformation of DOM (Andrews et al., 2000). Earlier research demonstrated the production of important oxidants such as hydroxyl radicals (OH), superoxide radicals (O_2^-), singlet oxygen ($^1O_2$), excited state DOM triplets and hydrogen peroxide (H_2O_2) (Fujii and Otani, 2017; Scully et al., 1996; Zhang et al., 2012; Dalrymple et al., 2010; Sun et al., 2015; Vaughan and Blough, 1998; Waggoner et al., 2017; Chu et al., 2015; Grandbois et al., 2008; McNeill and Canonica, 2016; Berg et al., 2019) through the photolysis of DOM in environmental waters. The production and consumption of these oxidants in natural waters is enhanced in the presence of trace metals, such as copper (Cu) and iron (Fe) through redox reactions (Jomova and Valko, 2011; Millero et al., 1991; Sharma and Millero, 1988; González-Davila et al., 2004; Millero et al., 1987; Moffett and Zika, 1983, 1987). High concentrations of these metals have been observed in different regions of the North Sea (Balls, 1985; Siems et al., 2024; Duinker and Nolting, 1982; Nolting, 1986; Mart and Nurnberg, 1986), so the estimation the photochemical production of reactive oxidants is of high importance in the present study to get more insights into the oxidative potential of this interface.

Biological activity can also influence photochemical processes in the surface of the oceans. Phytoplankton blooms refer to the rapid increase in microscopic algae in the upper layer of the sea, produced by both natural processes and nutrient enrichment from anthropogenic eutrophication (Dai et al., 2023). Recent scientific evidence revealed that the higher biological activity during a phytoplankton bloom and the subsequent algal decay have an impact on chemical properties and reactivity in the SML, as the organic matter (OM) accumulated in the air–sea interface can undergo photochemical changes due to excited triplet-state and radical-driven oxidation. For instance, there is a clear connection between marine microbiological processes and glyoxal production, especially in the terminal phase of an algal bloom (Williams et al., 2024). Nevertheless, integrated, compound-specific studies connecting the photochemistry of carbonyl compounds in different phases of algal blooms and the photooxidation potential of the SML remain insufficient.

In the present work, the photochemical activity of SML and ULW was investigated for samples collected during a mesocosm study in which a phytoplankton bloom was induced by the controlled addition of inorganic nutrients. The photochemistry of the seawater samples was assessed through the compound-specific concentration changes of carbonyl compounds before and after irradiation, alongside measurements of the photooxidation capacity to elucidate potential formation and degradation pathways of seawater samples at different bloom stages. The 17 carbonyl compounds analysed in the present study were acetophenone, acrolein, benzaldehyde, biacetyl, butanal, crotonaldehyde, glyoxal, heptanal, hexanal, isovaleraldehyde, methacrolein, methylglyoxal, methyl vinyl ketone (MVK), octanal, propanal, trans-2-hexenal and trans,trans-2,4-hexadienal. Even though acetaldehyde and acetone were initially also considered as target compounds, they were ultimately excluded from the final quantitative analysis since their calibration curves showed poor linearity, likely related

to their high volatility and potential background contamination from laboratory air. Formaldehyde was not analysed in the current study. Experimental evidence of enhanced photochemical activity of carbonyl compounds in the SML relative to the ULW is provided, particularly in periods of higher biological productivity, thereby offering new insights to integrate biological processes and photochemistry in the air–sea boundary.

2 Materials and methods

2.1 Seawater sampling during the field campaign

Ambient SML and ULW (40 cm depth) samples were collected during a mesocosm experiment conducted at SeasURface Facility (SURF), located at the Institute of Chemistry and Biology of the Marine Environment (ICBM) in Wilhelmshaven (Germany), between 18 May and 16 June 2023. SML samples were collected daily using the glass plate technique (Harvey and Burzell, 1972), while ULW samples were obtained via suction using a syringe connected to a polypropylene tube submerged to 40 cm.

A controlled phytoplankton bloom was induced through the stepwise addition of inorganic nutrients: silicate and phosphorous (19.8 and 1.2 $\mu mol\,L^{-1}$) were added on 26 May; silicate, nitrogen and phosphorous (10, 10 and 0.6 $\mu mol\,L^{-1}$) on 30 May, and nitrogen and phosphorous (5 and 0.3 $\mu mol\,L^{-1}$) on 1 June (Bibi et al., 2025). Based on chlorophyll *a* concentrations monitored in the ULW, three distinct bloom phases were defined:

(1) an initial pre-bloom phase, with lower chlorophyll *a* levels (average: 2.2 $\mu g\,L^{-1}$) prior to nutrient addition (18–26 May);

(2) a nutrient-induced bloom phase, (27 May to 4 June), characterized by a rapid increase in phytoplankton mass (average: 7.3 $\mu g\,L^{-1}$);

(3) a post-bloom phase, marked by the gradual decline in phytoplankton biomass (average: 1.8 $\mu g\,L^{-1}$) (5–16 June).

The concentrations of other phytoplankton pigments in the ULW samples followed similar trends to the ones reported for chlorophyll *a*. Concentrations of chlorophyll *c*, a photosynthetic pigment present in haptophytes ranged between 0.07 and 2.10 $\mu g\,L^{-1}$, peaking on 28 May, 1 and 3 June. Chlorophyll *b* and β-carotene were found between 0.04 and 0.40 $\mu g\,L^{-1}$, and 0.04 and 0.30 $\mu g\,L^{-1}$, respectively. Even though chlorophyll *b* and β-carotene seemed to have a minor contribution to the total phytoplankton mass, they also experienced an increase that reached maximum values between 1 and 3 June. Overall, the observed trends support the presence of a nutrient-driven phytoplankton bloom, which consisted of an initial dominance of *Emiliania huxleyi* (coccolithophore), followed by a subsequent growth of *Cylindrotheca Closterium* (diatoms) (Fig. 1) (Bibi et al., 2025). To further contextualize the biological development of the mesocosm, dissolved organic carbon (DOC) and particulate organic carbon (POC) concentrations were also analysed. DOC concentrations ranged from 254–583 $\mu mol\,L^{-1}$ in the SML, and from 207–373 $\mu mol\,L^{-1}$ in ULW. DOC concentrations increased during the phytoplankton bloom phase, and remained elevated in the post-bloom phase of the study. On the other hand, POC concentrations measured in the ULW samples were between 23 and 173 $\mu mol\,L^{-1}$, and their temporal trend along the mesocosm study was comparable to that of the chlorophyll *a* concentrations. In terms of bacterial abundance, which includes both free bacteria and bacteria-like material, it peaked in the post-bloom stage and ranged from 481×10^6 to 1468×10^6 in the SML, and from 245×10^6 to 1681×10^6 in the ULW. An enrichment factor (EF) of 1.3 ± 0.7 was found during the phytoplankton bloom. A detailed characterization of the biological parameters measured in this mesocosm study is provided by Bibi et al. (2025).

A detailed description of the mesocosm setup, and the operational and sampling protocols are also available in Bibi et al. (2025). Collected SML and ULW samples were stored in sterile bottles at −20 °C until laboratory analysis. All experiments were conducted using unfiltered samples in order to preserve as much as possible their natural complexity, and the results therefore reflect the combined photochemical processes involving both DOM and POM. A total of 20 different seawater samples, 12 from the SML and eight from the ULW, were selected to represent the three bloom phases (Table 1) for the investigations of carbonyl compound photochemistry. Their photochemical reactivity was analysed using methods described in the following sections. Samples from 20 May and 2 June were also considered for trace metals analysis.

2.2 Photochemical reactor

For carbonyl compound photochemistry investigations, ambient SML and ULW samples were irradiated for 5 h with a light source that simulated the actinic radiation in the sea surface. A jacketed, temperature-controlled (25 ± 0.5 °C) aqueous-phase cylindrical glass photoreactor (length: 9.5 cm, internal diameter: 6 cm) coupled with a thermostat (RCS, Lauda), were used to ensure constant temperature during irradiation. The solar simulator (LS0806, LOT-Quantum Design) consisted of a 1000 W Xenon lamp (LSB551, LOT-Quantum Design) coupled with an air mass filter (AM1-5G) that was positioned 20 cm away from the photoreactor (Fig. 2). This system has been designed to produce output power equivalent to 1 sun.

Samples were thawed a few hours prior to irradiation and introduced into the photoreactor without any pre-filtration to maintain to natural composition of OM. Due to sampling volume limitations in the mesocosm, particularly for the SML,

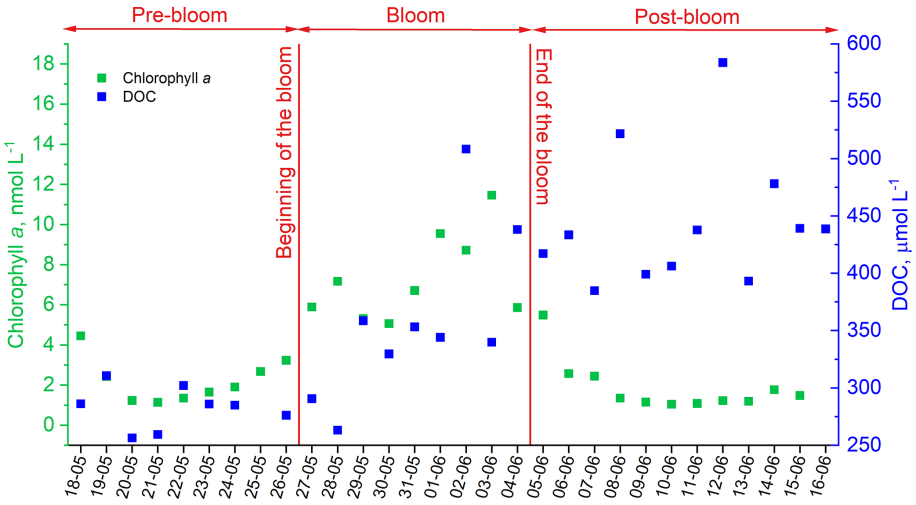

Figure 1. Chlorophyll *a* (monitored in the ULW) and DOC concentrations (monitored in the SML) along the mesocosm experiment. Based on the chlorophyll *a* concentrations, three phytoplankton bloom phases were defined: pre-bloom, bloom and post-bloom (adapted from Bibi et al., 2025).

Table 1. Overview of selected SML and ULW samples from the mesocosm analysed in this study for carbonyl compound photochemistry investigations.

Seawater sample name	Type of sample	Sampling date	Sampling time (local time)	Salinity (PSU)	Bloom phase
SML-5*	SML	20 May 2023	06:45	29.44	Pre-bloom
ULW-5*	ULW	20 May 2023	06:45	29.49	Pre-bloom
SML-7	SML	22 May 2023	06:27	29.59	Pre-bloom
SML-8	SML	23 May 2023	15:16	29.66	Pre-bloom
SML-11	SML	26 May 2023	06:20	29.87	Pre-bloom
ULW-11	ULW	26 May 2023	06:20	29.92	Pre-bloom
SML-12	SML	27 May 2023	15:35	29.91	Bloom
SML-13	SML	28 May 2023	07:10	29.95	Bloom
ULW-13	ULW	28 May 2023	07:10	30.00	Bloom
SML-15	SML	30 May 2023	05:50	30.16	Bloom
ULW-15	ULW	30 May 2023	05:50	30.29	Bloom
SML-17	SML	1 June 2023	06:14	30.25	Bloom
ULW-17	ULW	1 June 2023	06:14	30.30	Bloom
SML-18*	SML	2 June 2023	15:07	30.35	Bloom
ULW-18*	ULW	2 June 2023	15:07	30.38	Bloom
SML-23	SML	7 June 2023	05:30	30.86	Post-bloom
SML-24	SML	8 June 2023	14:59	31.01	Post-bloom
ULW-24	ULW	8 June 2023	14:59	31.04	Post-bloom
SML-27	SML	11 June 2023	05:30	31.31	Post-bloom
ULW-27	ULW	11 June 2023	05:30	31.35	Post-bloom

Adapted from Bibi et al. (2025).
* Samples used for trace metals analysis.

available volumes for irradiation were 125 mL for ULW and 50 mL for the SML. To ensure the comparability of both experimental conditions, absorbed photon fluxes were estimated using ferrioxalate actinometry (Sect. 2.5).

During irradiation, all samples were continuously stirred with a magnetic stir bar and a magnetic stirrer (IKA RAH basic 2, IKA) to maintain homogeneous mixing and consistent light exposure. Aliquots of 10 mL were collected at three time points: (1) before irradiation, (2) after 2.5 h, and (3) after 5 h of irradiation. For the ULW samples, two to three replicates were collected at each time point, and the final reported concentrations represent the average. Due to the limited sample volumes of SML (50 mL per irradiation), replicates of the SML samples could not be taken.

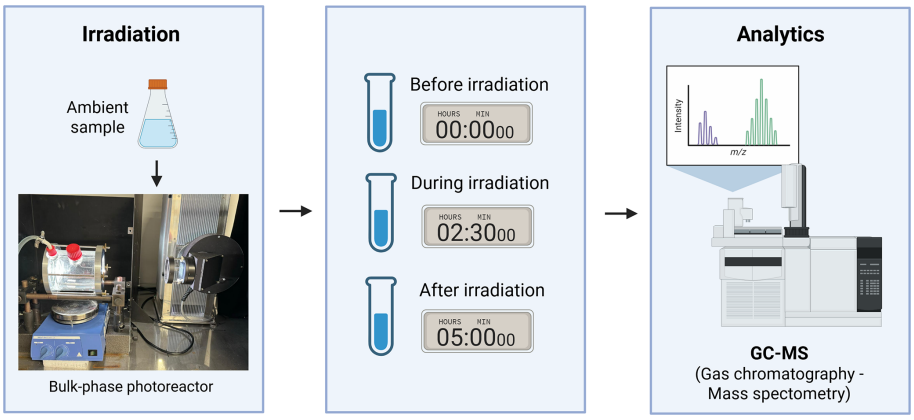

Figure 2. Workflow for the analysis of photochemical production of carbonyl compounds in the SML and ULW samples. Seawater samples were irradiated for 5 h, and aliquots of 10 mL were collected before the irradiation, after 2.5 and after 5 h. The aliquots were filtered, derivatized with o-(2,3,4,5,6-pentafluorobenzyl)hydroxylamine (PFBHA), extracted with iso-octane and analysed by GC-MS. Figure created with BioRender.com.

After the 5 h of irradiation, all the collected aliquots were either immediately processed together for the GC-MS analysis (Sect. 2.3), or stored at −20 °C for later electron paramagnetic resonance (EPR) analysis (Sect. 2.4) and trace metal analysis (Sect. 2.6).

2.3 Analytical method for the quantification of carbonyl compounds

The analysis of the target carbonyl compounds was carried out using a method based on derivatization with a o-(2,3,4,5,6-pentafluorobenzyl)hydroxylamine (PFBHA) reagent (> 99 %, Sigma Aldrich), followed by solvent extraction and gas chromatography-mass spectrometry analysis (GC-MS; Agilent 8890 GC coupled to Agilent 5977C GC/MSD, Agilent Technologies) in selected ion monitoring (SIM) mode. The GC was equipped with a HP-5MS column (30 m × 250 µm × 0.25 µm, Agilent Technologies). This method was originally developed for marine samples by van Pinxteren and Herrmann (2013), and further optimized by Rodigast et al. (2015) for application to other environmental samples (Rodigast et al., 2015; van Pinxteren and Herrmann, 2013).

Ultra-pure water (resistivity > 18 MΩcm) was used for the preparation of all the solutions described in Sect. 2.3–2.6, and for the cleaning of all the laboratory glassware. Process blanks were prepared for each seawater sample by dissolving synthetic sea salts (Sigma Aldrich) in ultra-pure water at salinities depending on values reported by Bibi et al. and shown in Table 1 (Bibi et al., 2025). After irradiation, 8 mL of the seawater samples from the 10 mL aliquots and the corresponding blanks were filtered using sterile 10 mL plastic syringes (Braun) and 0.2 µm PTFE membrane syringe filters (Pall). As internal standard, 100 µL of a 4.21 µg L^{-1} 2-(trifluoromethyl)benzaldehyde solution (98 %, Sigma Aldrich) prepared in ultra-pure water was added to each filtered sample. Afterwards, the derivatization solution was prepared by dissolving 30 mg of PFBHA (> 99 %, Sigma Aldrich) in 6 mL of ultra-pure water, and 200 µL were added to each of the samples. Then, 100 µL of hydrochloric acid (HCl) (37 %, CHEMSOLUTE) was added to accelerate the oxime formation. The prepared samples were allowed to react at room temperature for 18 h in the dark to guarantee that the derivatization process was completed, and that the oximes of the carbonyl compounds are formed.

After the 18 h of derivatization, iso-octane (> 99.5 %, Honeywell) was added as the extraction solvent (250–750 µL, depending on the expected OM load of each sample), followed by 20 µL of HCl (37 %) to enhance the extraction efficiency. Samples were then mixed manually for one minute and shaken with an orbital shaker (IKA VIBRAX VXR basic, IKA) at 1000 rpm for 30 min. From the resulting organic phase formed in the upper part of the mixture, 100 µL of the iso-octane layer was separated and placed into an insert in a GC autosampler amber vial (Agilent Technologies), and covered with a 9 mm PTFE screw (Agilent Technologies). Five µL of the extract were injected into the GC-MS system in pulsed splitless mode. The initial temperature of the oven was 50 °C, which was ramped to 210 °C.

The calibration was performed in duplicates using seven concentration levels (between 10 and 200 000 ng L^{-1},) of standard carbonyl compounds, which were derivatized and extracted following the same procedure explained above for seawater samples.

Quantification was performed by normalizing the peak areas of all the carbonyl compounds to the peak area of the internal standard. Data were acquired using Agilent Enhanced MassHunter software, and a chromatographic analysis was performed using Agilent MassHunter Qualitative Analysis 10.0 and Agilent MassHunter Quantitative Analysis

(for GCMS and LCMS). Relative compound-specific contributions were calculated from the quantified concentrations of each carbonyl compound relative to the total carbonyl concentration in each sample.

2.4 Analytical method for the estimation of the photooxidation capacity

The in situ spin-probing experiments were performed in a Bruker EMX Plus spectrometer in a 4103TM resonator. The resonator was coupled with an optical fibre accessory preceded by a 1.0 mm SCHOTT WG280 filter irradiated with a 150 W Xenon arc lamp (Hamamatsu Photonics). Samples were introduced in the resonator in glass capillaries with a wavelength cut-off at the UVC range (below 280 nm). The EPR spectrometer settings were the following: microwave frequency = 9.853 GHz, modulation amplitude = 1.00 G, magnetic field scan = 150 G, sweep time = 15 s, conversion time = 10 ms, time constant = 5 ms, and two accumulations. Spectra were acquired in the field delay mode at a 1 s scan delay. SML and ULW samples were added with the spin probe 1-hydroxy-3-methoxycarbonyl-2,2,5,5-tetramethyl pyrrolidine (CMH) (99 %, Noxygen), daily prepared at 10 mM in de-aerated ultra-pure water. Samples were added with 1 mM CMH, transferred to a 50 µL capillary tube, centered in the resonator, and subsequently irradiated for 30 min. The pH of the samples was not modified during the analysis and was kept as 8.4 ± 0.1. A Cr^{3+} signal-intensity marker ($g = 1.98$, Bruker) was simultaneously measured with all samples. The simulation of the spectra and radical quantification were performed in the SpinCount software package available in Xenon (Bruker Corporation). The accuracy of the calibration was confirmed using the signal of 2,2,6,6-tetramethyl-1-piperidinyloxyl (TEMPO) (99 %, Sigma-Aldrich). During the EPR measurements, it was confirmed that the resonator temperature remained stable at 298 K throughout the irradiation. The irradiation in the EPR was made using a 150 W Xenon lamp with radiation filters coupled to the resonator through an optical fibre, ensuring minimum transfer of infrared radiation and preventing sample heating.

Initially, SML and ULW samples were irradiated in the presence of 5,5-dimethyl-pyrroline N-oxide (DMPO), but no signals were observed over 30 min of irradiation, considering a limit of quantification of 100 nM. The samples were further irradiated in the presence of CMH. The CMH probe is known as an O_2^- radical probe due to its higher rate constant with these species ($1.2 \times 10^4\ M^{-1}\ s^{-1}$) when compared to other commonly used spin-trapping agents ($k(\text{DMPO} + O_2^-) = 0.8\text{–}50\ M^{-1}\ s^{-1}$). However, CMH also reacts with other reactive oxygen species (ROS) and one-electron oxidants, with rate constants of similar orders of magnitude (Gotham et al., 2020). The CMH autoxidation is also possible in the presence of CMH-reducible oxidants, such as metal ions, and it is therefore recommended that stock solutions are prepared in the presence of metal chelating agents. However, because the presence of complexing agents in seawater samples would affect their behaviour in photochemical experiments, daily stocks of CMH were prepared and a blank in ultra-pure water was measured before each analysis. The oxidation of CMH produced a nitroxide radical (here represented by CM radical) with a characteristic triplet EPR signal resulting from the hyperfine coupling between the unpaired electron of the CM radical and the nitrogen nucleus (aN).

Given the high lability of CMH, several precautions were taken to ensure the accuracy of the results. Several blanks were conducted to exclude the CMH autoxidation from the results observed in the presence of the irradiated SML samples. The rate of CMH autoxidation was subtracted from the rate of CM radical formation in the non-irradiated samples. This value was then normalized to the intensity of a Cr^{3+} marker signal ($g = 1.98$, Bruker) to guarantee signal homogeneity amongst experiments conducted over different days. We also observed small CM radical signals coming from the autoxidation of the stock solution of CMH prepared in ultra-pure water, which had minor contributions to the overall increase in the CM radical formation coming from the photoactivity of SML samples. Figure S1 in the Supplement illustrates the setup of the in situ EPR experiments.

2.5 Photon flux determination

As described in Sects. 2.3 and 2.4, two different setups were used for the photochemistry experiments. The absorbed photon fluxes in both experiments were determined using chemical actinometers, which are systems that contain a chromophore with well-characterized quantum yield. Photon fluxes were quantified by monitoring of the light-induced formation or degradation of the photolysis product of the chromophore (Rabani et al., 2021; Kuhn et al., 2004). In order to normalize the photon flux in each system and ensure comparability of the obtained results, photon fluxes were estimated for the photoreactor (I_{PR}) and for the capillary (I_{EPR}).

Photon flux in the photoreactor (I_{PR})

To estimate the photon flux in the photoreactor (I_{PR}), the well-established potassium ferrioxalate actinometer developed by Hatchard and Parker was used (Hatchard and Parker, 1956). The potassium ferrioxalate solution (6×10^{-3} M) was prepared following the detailed protocol described by Rabani et al., using ferric sulphate monohydrate (97 %, Sigma Aldrich), potassium oxalate monohydrate (99.98 %, Sigma Aldrich) and sulphuric acid (95 %, Fluka) (Rabani et al., 2021). As this actinometer is highly photosensitive and absorbs broadly between 200–600 nm, the preparation of the potassium ferrioxalate solution and the irradiation experiments were performed in a dark room only illuminated by red safety lamps. To represent the experimental conditions of both irradiated sample volumes (SML and ULW)

described in Sect. 2.3, the actinometry experiments were performed with two solution volumes: 50 and 125 mL. A detailed explanation of the experimental procedure and the steps for the estimation of the photon fluxes are provided in Sect. S1 in the Supplement. The determined photon fluxes were 2.7 µmol photons L^{-1} s^{-1} for 50 mL, and 2.8 µmol photons L^{-1} s^{-1} for 125 mL.

Photon flux in the capillary (I_{EPR})

The photon flux in the capillary for the EPR experiments (I_{EPR}) was determined using the method proposed by Moan et al. (1979) with the generation of $^1O_2$ from the irradiation of a porphyrin solution (Protoporphyrin IX–Target Mol) in the presence of 2,2,6,6-tetramethyl-4-piperidinol (TEMPOL) (98 %, Sigma-Aldrich) (Moan et al., 1979). This method was further optimized for its implementation to ambient seawater samples (Scheres Firak et al., 2026). The quantum yield for the production of singlet oxygen ϕ ($^1O_2$) by Protoporphyrin IX is 0.77 (Nishimura et al., 2020). The photon flux for the in situ EPR experiments was estimated as $(9 \pm 2) \times 10^{-9}$ mol photons L^{-1} s^{-1} using the irradiation of Protoporphyrin IX solution ($c_0 = 10$ µM) in the presence of TEMPOL ($c_0 = 100$ µM).

2.6 Analytical method for the measurement of trace metals

Trace concentrations of iron (Fe) and copper (Cu) were measured directly from the seawater samples using a benchtop total reflection X-ray fluorescence (TXRF) S4 T-STAR spectrometer (Bruker AXS). Five µL of seawater sample were spiked with 5 ng (50 ng for samples collected on 11 June) internal standard of Sc/Co in ultra-pure water solution, on a TXRF quartz carrier. Before the measurement, the TXRF carriers were allowed to dry at 80 °C on a hot plate for about 5 min. Each analysis lasted typically 500 s. X-ray data acquisition and quantification of elemental concentrations was performed using the SPECTRA 6.2 software. This method was originally developed by Fomba et al. for the investigation of trace metal concentrations in particulate matter (PM) and cloud water (Fomba et al., 2013, 2020), and further optimized for its application to seawater samples in the present study. To represent the three stages of the phytoplankton bloom, we analysed the SML and ULW samples collected on 20 May (pre-bloom) and 2 June (bloom).

2.7 Text management

ChatGPT (Open AI, 2025) was used for language polishing assistance.

3 Results and discussion

3.1 Concentrations of carbonyl compounds in irradiated samples under bloom and non-bloom conditions

Figure 3 illustrates the individual concentrations in the seawater samples of the 17 carbonyl compounds in four categories: SML before irradiation (Fig. 3A), SML after 5 h of irradiation (Fig. 3B), ULW before irradiation (Fig. 3C), and ULW after 5 h of irradiation (Fig. 3D). Relative changes induced by irradiation (% increase/decrease) in carbonyl compound concentrations are shown in Fig. S3 in the Supplement to facilitate comparison of photochemical responses across compounds. The observed photochemical transformations of carbonyl compounds likely arise from the combined processing of both the DOM and POM (including intact cells, cellular debris, and particulate biological material potentially released during freeze–thaw cycles). As a result, the reported photochemical rates represent the integrated responses of the total OM pool present in the SML and in ULW.

Carbonyl concentrations varied considerably between SML and ULW, and across bloom phases. Total carbonyl concentrations were generally higher in samples collected during the bloom phase compared to the pre- and post-bloom phases, with exception of the SML sample collected on 8 June (Fig. 3A). In that day, the concentration of propanal before irradiation reached 4027 nmol L^{-1}, a value significantly higher than in the irradiated counterpart (Fig. 3B). Propanal and hexanal where the most abundant compounds during the bloom phase, suggesting that their formation is favoured under conditions of high biological productivity. Propanal exhibited remarkably higher concentrations with respect to other species, particularly in the SML during the bloom and post-bloom phases. This suggests that propanal may represent an important, yet previously underrecognized, contributor to the carbonyl pool at the air–sea interface. Further targeted studies with increased temporal resolution and replication are required to better understand the specific mechanisms driving its massive production in these conditions.

Throughout all bloom phases, the SML (Fig. 3A and B) had consistently higher concentrations than the ULW samples (Fig. 3C and D) both before and after irradiation, despite similar photon fluxes were confirmed by actinometry (see Sect. 2.5). Before irradiation, values in the SML (Fig. 3A) ranged from 201 to 762 nmol L^{-1} in the pre-bloom phase, 984–4591 nmol L^{-1} in the bloom phase, and 647–4894 nmol L^{-1} in the post-bloom phase; while in the ULW (Fig. 3C) they were significantly lower (e.g., 136–366 nmol L^{-1} in the bloom phase). After 5 h of irradiation, the concentrations of carbonyl compounds increased further, reaching up to 6026 nmol L^{-1} in the SML (Fig. 3B) during the bloom phase and 419 nmol L^{-1} in the ULW (Fig. 3D). This suggests the light-driven production of aldehydes and

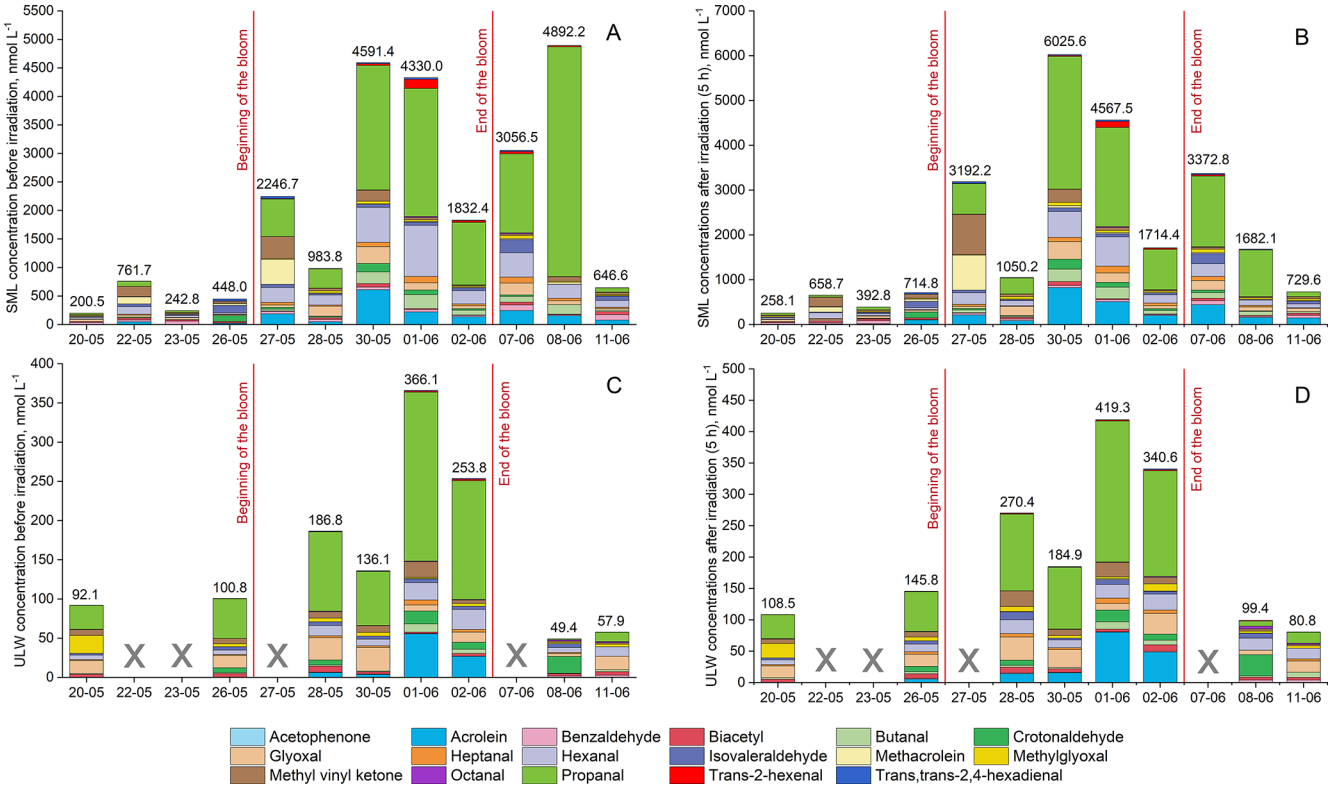

Figure 3. Speciation of 17 carbonyl compounds in SML samples before irradiation **(A)** and after 5 h of irradiation **(B)**, and ULW samples before irradiation **(C)** or after irradiation **(D)**. The red lines separate the three phases of the mesocosm experiment. ULW samples collected on 22 May, 23 May, 27 May and 7 June were not available for their analysis.

ketones, probably via direct photolysis, photochemical oxidation or photosensitized reactions. These observed SML enrichments for all the aldehydes and ketones under evaluation are in agreement with previous studies for glyoxal, methylglyoxal, propanal and butanal (Zhou and Mopper, 1997; van Pinxteren and Herrmann, 2013), and provide novel insights on the behaviour of a larger pool of carbonyl compounds with potential relevance in the marine environment, such as MVK or methacrolein. Overall, our findings indicate that the unique physical and chemical environment in the surface of the sea, richer in organic compounds compared to ULW, favours the production of these carbonyl compounds.

These trends could be attributed to several factors, such as the diverse chemical composition, reactivity, optical properties and availability of the OM in the different water layers. Surface waters are typically characterized by their enrichment in more photoreactive and autochthonous OM, contrasting with the more degraded and refractory compounds in the underlying waters (Wagner et al., 2020; Yang et al., 2022).

Our data shows higher concentrations of carbonyl compounds generally during the phytoplankton bloom phase (Fig. 3), suggesting a strong direct or indirect influence of biological productivity on the availability of precursors for the production of aldehydes and ketones. Higher concentrations were partly found in the post-bloom compared to the pre-bloom. This pattern is in agreement with the parallel increase of the DOC levels with the phytoplankton abundance in the bloom phase, and with how these levels also remained high in the post-bloom phase (Fig. 1). Generally, high variability in the concentrations of humic-like compounds and in the ratios of labile/refractory compounds were found through the duration of the mesocosm, which supports the idea of bloom-dependent OM transformations (Thölen et al., 2026; Zöbelein et al., 2026). Fresh biological material produced during phytoplankton blooms is a source of photochemically-active OM. For instance, *Emiliania huxleyi*, a specie of photosynthetic coccolithophore that dominated at the early bloom phase (Bibi et al., 2025), is characterized by its efficient photochemical production of isoprene, a volatile precursor of several carbonyl compounds (Shaw et al., 2003; Sinha et al., 2007). Comparable trends have been observed in marine diatoms and dinoflagellates (Moore et al., 1994; Milne et al., 1995), which may explain the formation of carbonyl compounds in marine environments. Likewise, the photochemical production of aldehydes and ketones from lipids derived from *Chaetocerus pseudocurvisetus* has been recently demonstrated (Penezic et al., 2023). Furthermore,

the major fatty acids from other diatoms like *Phaeodactylum triconutum* might be precursors of hexanal through oxidation reactions (Schobert and Elstner, 1980). Oxidative stress during blooms and photochemical degradation of OM are linked to the massive production of ROS (Hansel and Diaz, 2021), which may trigger processes like isoprene oxidation and lipid peroxidation, leading to the release of aldehydes and ketones.

Altogether, this experimental evidence indicates that phytoplankton blooms influence not only the biological activity in seawater but may also modulate abiotic processes, particularly in the SML, by changing OM chemical composition and reactivity.

3.2 Photochemical production rates under bloom and non-bloom conditions

We investigated the photochemical formation and degradation rates of the 17 carbonyl compounds in both SML and ULW samples (Figs. 4 and 5, expressed in $\mathrm{mol\,mol(DOC)^{-1}\,L^{-1}\,h^{-1}}$). In the three phases of the mesocosm study, the carbonyl compounds in the SML samples (red) presented consistently higher photochemical production rates than in the ULW (blue). These findings are likely due to the enrichment of photochemically-active compounds and surface-active molecules, such as lipids, fatty acids and aromatic compounds in the SML; which contrast with the more processed and aged OM typically present in the ULW (Sect. 3.1).

The photochemical production rates in the SML and ULW of the 17 carbonyl compounds were classified in two major categories, based on how their time-resolved photochemistry was influenced by the phytoplankton bloom:

Photochemistry influenced by the bloom

Ten out of 17 compounds showed enhanced photochemical formation or degradation in the SML during the phytoplankton bloom: MVK, methacrolein, glyoxal, methylglyoxal, acrolein, crotonaldehyde, heptanal, biacetyl, hexanal and trans-2-hexenal.

These trends suggest an influence of the stage of the phytoplankton bloom in the photochemical activity of these carbonyl compounds in the SML, presumably due to the elevated concentrations of photochemically-active precursors and higher oxidative stress. Even though the overall DOC concentrations remained relatively stable during the bloom and post-bloom phases of the mesocosm study (Fig. 1), the fresher and more photoreactive nature of the phytoplankton-derived CDOM and photosensitizers in the bloom phase seemed to enhance the generation of excited triplet-state DOM and ROS, promoting the photochemical production of these carbonyl compounds in the SML.

Interestingly, the temporal behaviour of the production rates of isoprene oxidation products had a characteristic pattern: methacrolein (Fig. 4A) and MVK (Fig. 4B), both primary isoprene products, had peak productions in the early stage of the bloom; while glyoxal (Fig. 4C), methylglyoxal (Fig. 4D) and acrolein (Fig. 4E), all secondary isoprene products, dominated the later stage of the bloom. This temporal pattern suggests a dynamic photochemical response in the SML regarding isoprene formation likely driven by the changes in the composition of OM throughout a phytoplankton bloom. Isoprene is a trace gas produced both photochemically at the sea surface (Wang et al., 2023) and biologically by marine phytoplankton (Moore et al., 1994; Simó et al., 2022; Sinha et al., 2007; Ciuraru et al., 2015). In seawater, it is typically present in concentrations of few $\mathrm{pmol\,L^{-1}}$ (Conte et al., 2020; Milne et al., 1995). In the atmosphere, isoprene can undergo an oxidation reaction, for example, with OH radicals, NO_3 radicals or O_3 (Atkinson, 2000), yielding MVK and methacrolein as primary products, and acrolein, glyoxal and methylglyoxal as secondary products. Indeed, nearly 50 % of glyoxal and more than 70 % of methylglyoxal in the atmosphere are estimated to originate from isoprene oxidation (Fu et al., 2008). The aqueous-phase photooxidation of isoprene by OH radicals has also been demonstrated (Huang et al., 2011), and due to the intense solar radiation and the presence of OH radicals in the SML (Zhou and Mopper, 1990a), isoprene-derived species such as MVK, methacrolein, acrolein, glyoxal and methylglyoxal are likely formed in this environment. Oxidation of acetone, glycolaldehyde and acetaldehyde also yields glyoxal and methylglyoxal (Walker et al., 2022); indeed, acetone has been reported to be responsible for more than 7 % of the global production of methylglyoxal (Fu et al., 2008). There is experimental evidence of marine production of acetaldehyde and acetone (de Bruyn et al., 2011; Kieber et al., 1990; Sinha et al., 2007; Zhu and Kieber, 2018; Millet et al., 2010; Wang et al., 2019; Mopper et al., 1991), and the unique environment of the SML could facilitate their transformation into other carbonyl compounds. Additionally, OH-driven oxidation or ozonolysis of hydrocarbons, such as 1,3-butadiene, benzene, toluene, acetylene and xylene, has been reported to yield carbonyl compounds like acrolein, glyoxal, methylglyoxal and biacetyl in the gas phase (Tuazon et al., 1999; Jaoui et al., 2025). Aromatic hydrocarbons, such as benzene, toluene, acetylene and xylene, also undergo OH-initiated oxidation in the atmosphere primarily through ring-cleavage, yielding glyoxal, methylglyoxal and biacetyl (Volkamer et al., 2001; Tuazon et al., 1986; Fu et al., 2008). In summary, these well-characterized degradation pathways in the gas phase provide useful mechanistic analogues for understanding possible photochemical transformations of these compounds in the SML.

Phytoplankton and algae produce polyunsaturated fatty acids (PUFAs) and saturated fatty acids, which degrade via reactions with radicals and lead to the formation of carbonyl compounds. Peroxidation of lipids is a source of a diverse pool of carbonyl compounds including acrolein, butanal, crotonaldehyde, glyoxal, hexanal, propanal, and trans-2-hexenal

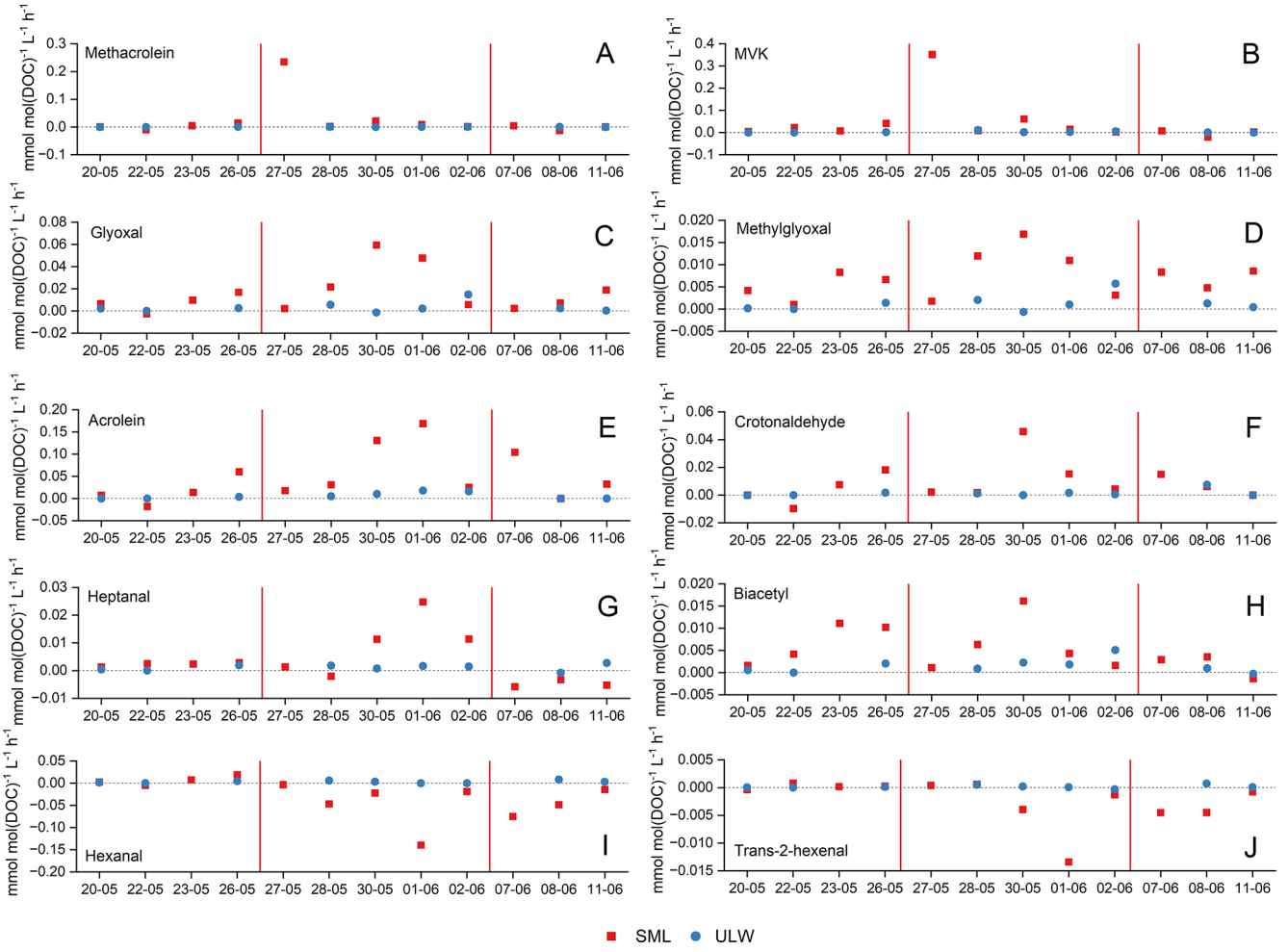

Figure 4. Comparison of photochemical formation and degradation rates of methacrolein **(A)**, MVK **(B)**, glyoxal **(C)**, methylglyoxal **(D)**, acrolein **(E)**, crotonaldehyde **(F)**, heptanal **(G)**, biacetyl **(H)**, hexanal **(I)** and trans-2-hexenal **(J)** in the SML (red) and in ULW (blue). The red vertical lines separate the three phases of the mesocosm study: pre-bloom (20 to 26 May), bloom (27 May to 2 June) and post-bloom (8 to 11 June). Photochemical production and degradation rates in the ULW samples on an expanded scale, including error bars that reflect analytical and sample-handling uncertainties, are shown in Fig. S4 in the Supplement.

(Uchida et al., 1998; Zhou et al., 2014; Onyango, 2012; Kato et al., 2022; Wu and Lin, 1995). For instance, the enzymatic breakdown of linoleic acid by lipoxygenase and hydroperoxide lyase in marine algae yields hexanal (Boonprab et al., 2003). In addition to that, trans,trans-2,4-hexadienal may also form as an oxidation product of fatty acids (Ferrario et al., 1985).

Enhanced photochemical degradation of hexanal (Fig. 4I) and trans-2-hexenal (Fig. 4J) was also observed during the bloom phase. Both compounds presented the highest photochemical degradation rates on 1 June, $-0.14\,\mathrm{mmol\,mol(DOC)^{-1}\,L^{-1}\,h^{-1}}$ for hexanal and $-0.01\,\mathrm{mmol\,mol(DOC)^{-1}\,L^{-1}\,h^{-1}}$ for trans-2-hexenal. This coincides with the expected generation of large quantities of ROS, such as OH radicals, O_2^- and $^1O_2$ linked to oxidative stress in phytoplankton blooms (Cho et al., 2022). These species would be massively available during the bloom to degrade hexanal and trans-2-hexenal, a process similar to what has been observed in the gas phase (Jiménez et al., 2007; Tadic et al., 2001).

In general, carbonyl compounds can be degraded by photolysis and radical-driven oxidation (Atkinson, 2000; Epstein et al., 2013; Tilgner and Herrmann, 2010), processes that are likely intensified by the high concentrations of OM and strong solar radiation characteristic of the SML. In the gas phase, photolysis and oxidation by OH radicals have been estimated to account for up to 76 % of glyoxal and 82 % of methylglyoxal removal (Fu et al., 2008). Likewise, tropospheric losses of hexanal and trans-2-hexenal are also mainly attributed to reactions with OH radicals (Jiménez et al., 2007). OH radicals react with aldehydes and ketones via hydrogen abstraction from the -CHO group (Atkinson, 2000), and as these radicals are continuously formed in seawater via photochemical reactions involving CDOM (Zhou

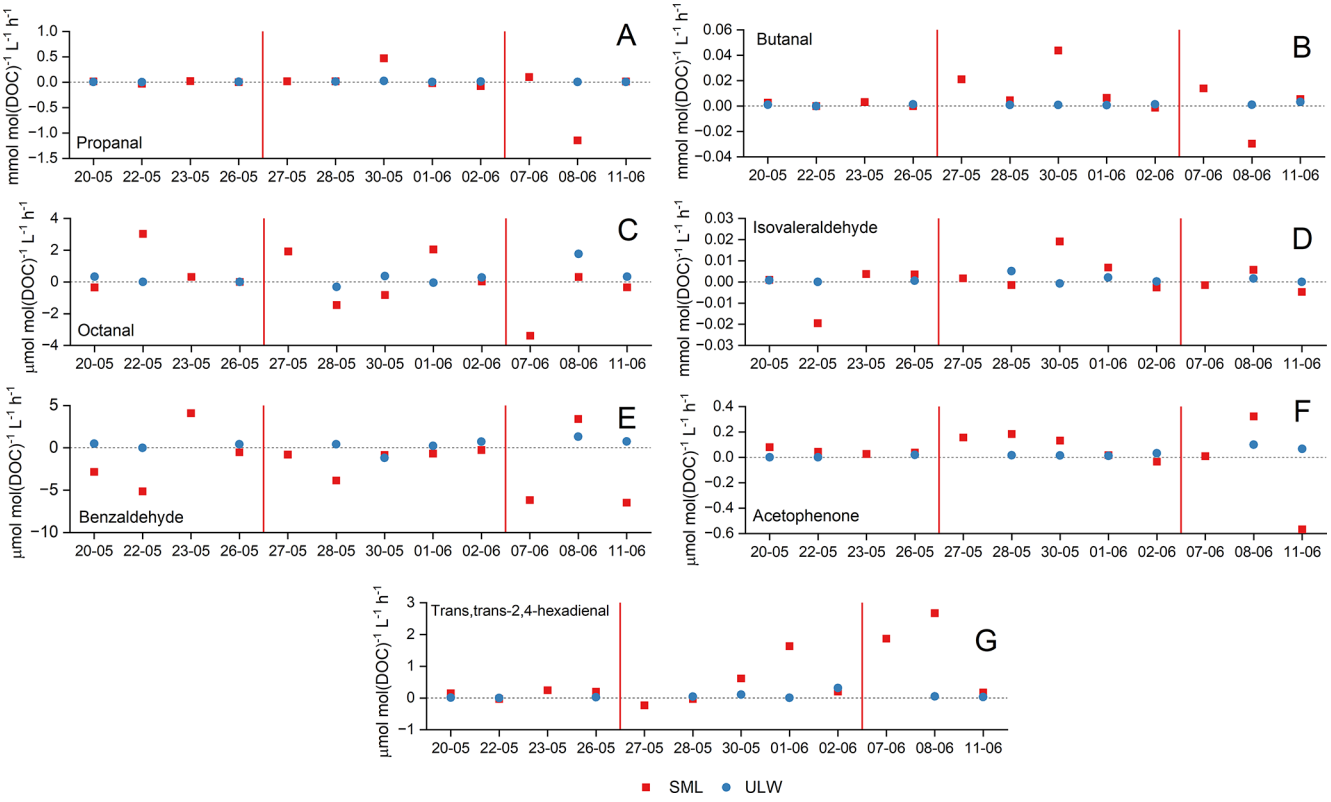

Figure 5. Comparison of photochemical formation and degradation rates of propanal **(A)**, butanal **(B)**, octanal **(C)**, isovaleraldehyde **(D)**, benzaldehyde **(E)**, acetophenone **(F)** and trans,trans-2,4-hexadienal **(G)** in the SML (red) and in ULW (blue). The red lines separate the three phases of the mesocosm study: pre-bloom (20 to 26 May), bloom (27 May to 2 June) and post-bloom (8 to 11 June). Photochemical production and degradation rates in the ULW samples on an expanded scale, including error bars that reflect analytical and sample-handling uncertainties, are shown in Fig. S4.

and Mopper, 1990a), OH-oxidation is a significant sink of carbonyl compounds in the SML.

Photochemistry independent of the bloom:

The photochemistry of seven out of the 17 compounds showed no clear influence of the bloom: butanal, isovaleraldehyde, benzaldehyde, trans,trans-2,4-hexadienal, octanal and acetophenone (Fig. 5). These compounds may be possibly derived from a mixture of both biogenic and anthropogenic sources, with less influence of the bloom intensity compared to the compounds in the first category.

Propanal (Fig. 5A) and butanal (Fig. 5B) were the most photochemically active compounds in this category. They are small aldehydes commonly linked to the oxidation of larger organic molecules, which could explain their abundance in the different phases of the study. The photochemical activity of the aromatic carbonyls, benzaldehyde (Fig. 5E) and acetophenone (Fig. 5F), peaked in the pre- and post-bloom phases and was relatively lower than for the other compounds. This could suggest an increased presence of humic-like DOM derived from anthropogenic activity or terrestrial sources, which is less labile but still photochemically-active. The photooxidation of aromatic hydrocarbons can lead to the production of acetophenone and benzaldehyde (Ehrhardt and Petrick, 1984; Ehrhardt et al., 1982). Aromatic hydrocarbons are generally considered anthropogenic, but marine phytoplankton has also been reported as a source particularly under oxidative stress (Rocco et al., 2021). In addition to aromatic hydrocarbons, the photodegradation of polystyrene nanoparticles by OH radicals or ozone generates acetophenone and benzaldehyde (Davidson et al., 2005; Bianco et al., 2020; Fabbri et al., 2023). The presence of these compounds in the seawater samples suggests plastic contamination, which in nature also contributes to the release of carbonyl compounds. However, the concentrations of acetophenone and benzaldehyde accounted only for up to 2 % of the total sum composition of carbonyl compounds in SML samples, so these sources appear to be minor. The production of octanal (Fig. 5C) and trans,trans-2,4-hexadienal (Fig. 5G) is also comparatively lower, likely because it requires the preservation of longer carbon chains and more complex structures.

In general, the high photochemical production rates observed in the later stage of the bloom and during the post-bloom phase of the experiment may be explained by the pho-

tochemical degradation of lipids and humic-like compounds as precursor molecules, which could represent a higher proportion of the OM due to the beginning of the phytoplankton decay from viral cell lysis, senescence o grazing (Rochelle-Newall et al., 1999).

To facilitate comparison with existing literature, the non-normalized rates were also calculated and are provided in Figs. S8 and S9 in the Supplement. The findings for glyoxal and methylglyoxal in non-bloom phases are consistent with published photochemical production rates from SML samples collected in the Bahamas, Delaware Bay (USA) and Biscayne Bay (USA), which range between 0.75 and 5.8 $\mathrm{nM\,h^{-1}}$ for glyoxal, and 0.3 and 2.5 $\mathrm{nM\,h^{-1}}$ for methylglyoxal (Mopper and Stahovec, 1986; Zhou and Mopper, 1997). On the other hand, the higher photochemical formation rates found during the bloom phase for these two compounds were comparable with those reported by Zhou and Mopper for SML samples (up to 15.5 $\mathrm{nM\,h^{-1}}$ for glyoxal and 9.7 $\mathrm{nM\,h^{-1}}$ for methylglyoxal), collected in the Biscayne Bay in the presence of foam on the sea surface (Zhou and Mopper, 1997). Likewise, rates of photochemical formation reported in the ULW align well with those determined in the present study (Zhu and Kieber, 2018; Zhou and Mopper, 1997). Higher photochemical activity in short-chain aldehydes was observed, compared to literature values: Zhou and Mopper reported formation rates between 1.3 and 7.4 $\mathrm{nM\,h^{-1}}$ for C_3 aldehydes, and between 0.4–4.2$\mathrm{nM\,h^{-1}}$ for C_4 aldehydes (Zhou and Mopper, 1997). Despite the lower magnitudes compared to the present study, Mopper and Stahovec also observed photochemical degradation of propanal ($-0.75\,\mathrm{nM\,h^{-1}}$) in surface water samples from the Biscayne Bay (Mopper and Stahovec, 1986). Apparent quantum yields (AQYs) were calculated from the measured photoproduction rates and the absorbed photon fluxes (Sect. S6 in the Supplement). Because the experiments were conducted using unfiltered samples, the derived AQYs represent effective photochemical efficiencies of the total OM pool, including both DOM and POM. The results demonstrate that the SML is a more photochemically-efficient environment compared to ULW, particularly during the bloom phase. No systematic relationship was observed between AQYs and DOC concentrations (Fig. S5 in the Supplement), suggesting that OM abundance alone does not control the efficiency of these photochemical processes.

By connecting phytoplankton bloom dynamics and the temporal trend of the photochemical products, our results stress the crucial role of the SML as a dynamic air–sea boundary and its potential implications for the production of VOCs to the marine atmosphere. These findings are of high relevance for refining atmospheric models in the marine environment, as climate change is projected to cause shifts in nutrient and sunlight availability, thereby influencing phytoplankton blooms and marine carbon cycling (Thomalla et al., 2023; Dai et al., 2023).

3.3 Photooxidation capacity under bloom and non-bloom conditions

Investigations of photooxidation capacity in the seawater samples are essential to understand how the sunlight-driven production of reactive intermediates influences the transformation of OM and the subsequent formation of VOCs. The photooxidation capacity of SML and ULW samples was tested using a radical probe in EPR experiments. Since radicals are short-lived species, they require probes or spin-trapping agents that react with radicals to form stable paramagnetic species that can be further detected with an EPR spectrometer. Nitroxides such as DMPO and CMH are respective examples of spin-trapping agents and spin probes typically used to investigate the formation of radicals in ambient samples (Briedé et al., 2005; Arangio et al., 2016).

As seen in Fig. 6, the formation of CM radicals occurred in all samples and increased linearly during the monitored time. These values were then represented in bar plots that illustrate the overall budget of oxidants photochemically generated in the samples (Fig. 7).

As presented in Fig. 7, the overall photochemical oxidation capacity of the samples did not seem to be affected by the addition of nutrients. It was also, on average, similar for both SML and ULW samples, with values around 34 $\mathrm{\mu M\,s^{-1}}$. To evaluate whether these results reflect enhanced photochemical reactivity or simply the highest abundance of OM the measured photooxidation capacities were compared to DOC concentrations (Fig. S7 in the Supplement). No systematic correlation was found, indicating that the observed results cannot be explained solely by the abundance of OM. While nutrient levels can indirectly influence the redox capacity of seawater samples through phytoplankton blooms, they ultimately did not appear to control it. The oxidation potential of the samples seemed to be primarily determined by the presence and availability of electron donors and acceptors. Although the complexity of the mesocosm samples makes it difficult to attribute the oxidation properties to individual species, a dominant class of redox-active compounds known to be present in seawater are metal ions. Nutrient levels, while impacting the concentrations of individual metal ions, do not dictate the overall budget of oxidizers, which is mostly modified through atmospheric deposition, agricultural and industrial runoff, and discharges from oil and gas platforms (Wurl et al., 2017). A study investigating the presence of nutrients and metals in waters of the North Sea attributed the highest metal content to the waters of the German Bight, source of the water used in the mesocosm study. Concentrations of redox-active metals, such as copper (Cu) and iron (Fe), were measured in values as high as 749 and 150 $\mathrm{ng\,L^{-1}}$ in this region (Siems et al., 2024). These metals have pronounced photochemical activity, and synergistic effects are known to play significant roles in their redox chemistry (Lueder et al., 2020; Deguillaume et al., 2005).

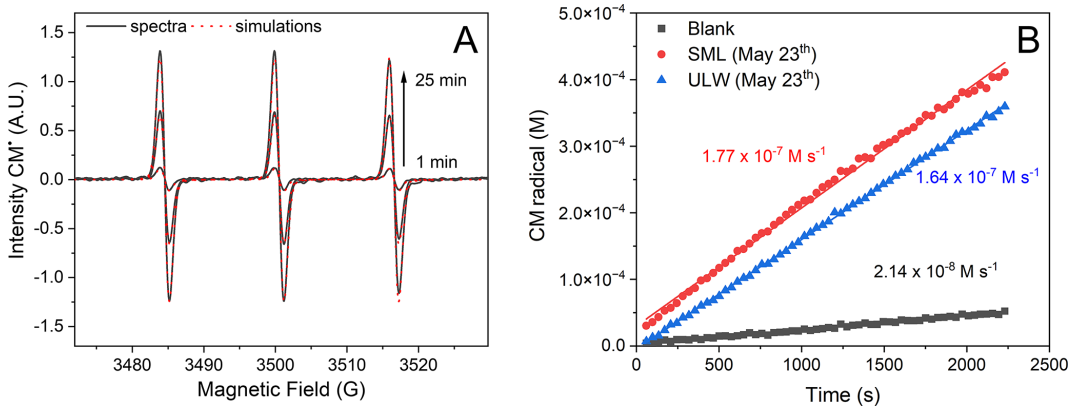

Figure 6. **(A)** EPR spectra of CM radicals at different irradiation times. Spectral parameters: aN = 16 G, $g = 2.0056$. **(B)** Profile of CM radical formation over time for blank, SML, and ULW samples. The blank in **(B)** represents the CM radical formation in the absence of light. The resultant signals were subsequently plotted as a function of the irradiation time, and fitted to a linear regression to get the rate of CM radical formation over time. The formation of CM radical was normalized by the ratio between I_{EPR} and I_{PR}. This normalization procedure yields CM radical formation rates that account for the energy input of the photoreactor, which is circa 300 times greater than the energy input in the in situ EPR experiments due to the smaller sample volumes required for the EPR measurements.

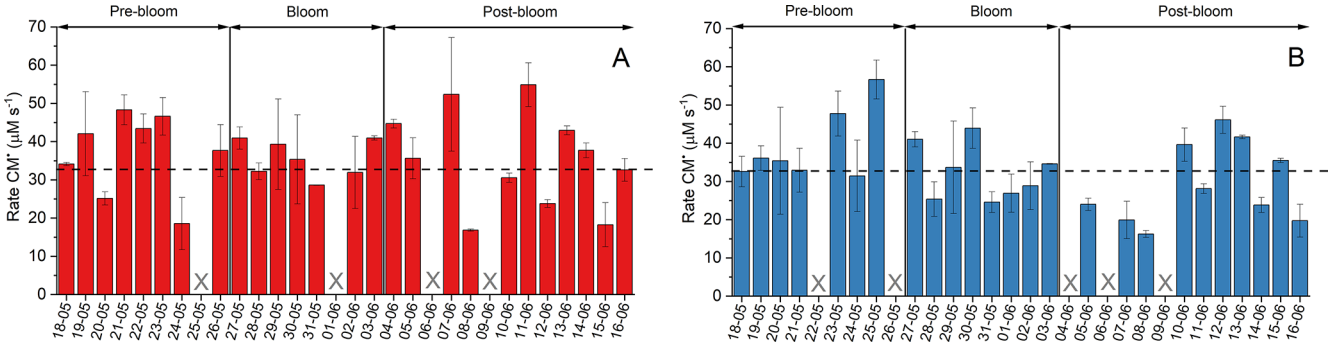

Figure 7. The overall CM radical formation in different samples after photon-flux correction for SML **(A)** and ULW **(B)** samples. The dashed line represents the mean CM radical formation rate considering all samples.

To evaluate if these processes might have an influence in our observed results for the mesocosm study, the concentrations of Cu and Fe in SML and ULW samples were quantified. TXRF measurements demonstrated the presence of Cu and Fe in the pre-bloom phase (20 May) and during the bloom (2 June). Cu concentrations in the SML and in the ULW were 0.3 and 0.2 µmol L^{-1} on 20 May, and 0.5 and 0.3 µmol L^{-1} on 2 June. Fe concentrations in the SML and in the ULW were 1.2 and 1.0 µmol L^{-1} on 20 May, 9.2 and 1.8 µmol L^{-1} on 2 June. Compared to those reported by Siems et al., we found slightly lower concentrations of Cu and much higher concentrations of Fe. As expected, the distribution of redox-active trace elements in the SML and ULW samples was relatively uniform. Previous studies have demonstrated that metal concentrations only decrease at higher water depths (Siems et al., 2024). These trace metal concentrations might contribute to the high observed redox activity of the samples in the in situ EPR experiments. However, further targeted studies are needed to quantify the relative role of metal ions and other redox-active components in seawater photooxidation.

As shown in Sect. S3 in the Supplement, control experiments were conducted to verify the activity of Fe and Cu chloride salts, and a great contribution of Cu(I) and Cu(II) in the formation of CM radicals was observed, with formation rates reaching 16 µM s^{-1} in the photolysis of a 500 nM CuCl solution. Fe(II) solutions showed no photoactivity, while Fe(III) showed a small contribution to CM radical formation, with maximum formation rates of 0.2 µM s^{-1}. Although Cu ions were detected in the TXRF analysis, their presence alone does not account for the total observed photooxidation capacity of the samples. Considering the high reaction rates between CMH and O_2^-, and the absence of signals in the presence of DMPO, the formation of O_2^- is a strong candidate for the remaining CM radical formation rates. Measured formation rates calculated from the steady state concentrations of O_2^- radical considering CDOM photochemistry in natural ocean waters can reach 480 nM h^{-1} (Hansard et al., 2010),

while OH radical formation rates reach 110 nM h^{-1} (Mopper and Zhou, 1990). In the EPR experiments, direct electron transfer from excited photosensitizers can also influence the results and contribute to the rate of CM formation.

Although the control experiments with Fe and Cu chloride salts indicate that Cu has a stronger effect on CMH oxidation than Fe, metal complexation significantly modulates the redox properties and the solubility of both Fe(III) and Cu(II) in seawater. In general, photoreduction is enhanced in the presence of ligands that form photoactive inner-sphere complexes and enable ligand-to-metal charge transfer (LMCT). While ligands, such as oxalate, are known to significantly increase the quantum yields for the metal reduction, this effect is much weaker for ligands with a lower stability constant (Sun et al., 1998). The solubility of Fe and Cu ions in ocean water is generally reduced in the absence of organic ligands due to the formation of hydroxy-oxo insoluble species promoted at typical seawater pH levels. Therefore, the presence of OM enhances the photochemistry of Fe and Cu in seawater by increasing the solubility of ions (Millero, 1998; Calza et al., 2014). However, OM itself comprises fulvic and humic acids, which have photosensitizing properties. Direct photosensitization processes can be suppressed when these photosensitizers are bound to Fe, since LMCT mechanisms will be favoured (Calza et al., 2014). Consequently, the overall effect of Cu and Fe complexation is very complex. While attributing the observed photooxidation capacity to a specific decrease or increase in redox activity would require dedicated metal speciation and ligand characterization, the stable CMH photooxidation rates observed across bloom phases and between the SML and ULW suggest that changes in total Fe concentrations did not exert a dominant control on the measured redox activity under the investigated conditions.

3.4 Implications for the ocean and the atmosphere

Carbonyl compounds can be transferred from the sea surface to the atmosphere due to their volatile nature, making air–sea exchanges of high relevance in their marine biogeochemical cycling. In general, the transfer of a compound from the liquid phase to the gas phase can be described using the two-layer model, which has been widely applied in the literature to estimate air–sea fluxes (Liss and Slater, 1974). In this model, the equilibrium concentrations of a compound in the gas (c_{sg}) and in the liquid (c_{sl}) at the interface are related through its apparent partition coefficient (H, in M atm^{-1}), as expressed in Eq. (1):

$$H = \frac{c_{sl}}{c_{sg}}, \quad (1)$$

From the photochemical formation rates measured in the SML and the apparent partition coefficients (Table 2) compiled by Sander (Sander, 2023), the rates of transfer of photochemically produced carbonyl compounds from the SML (c_{sl}) to the gas interface (c_{sg}) were estimated. Constant SML thickness of 100 µm and temperature of 298 K were assumed for the calculations. Isovaleraldehyde and trans,trans-2,4-hexadienal were not considered due to the lack of published partition coefficient data. The rates of transfer were calculated excluding the samples in which photochemical degradation rather than formation was observed; thus, we report no values for benzaldehyde and hexanal in the bloom phase. The non-bloom values in the table include both the pre-bloom and post-bloom phases of the mesocosm. A detailed explanation of the steps for the estimation of the rates of transfer to the gas interface are provided in Sect. S5 in the Supplement.

The estimated rates of transfer of photochemically-produced carbonyl compounds from the SML to the atmosphere according to equilibrium partitioning were generally higher during the bloom phase for the majority of the compounds, namely acrolein, biacetyl, butanal, crotonaldehyde, glyoxal, heptanal, methacrolein, methylglyoxal, MVK, propanal and trans-2-hexanal. This trend suggests that biological processes in the SML may also enhance the emission of VOCs to the atmosphere. However, for soluble compounds like glyoxal and methylglyoxal, their transfer into the gas phase is relatively low compared to other compounds with lower apparent partition coefficients. Although these compounds are photochemically produced in the SML, the net exchange direction is presumed to be predominantly from the atmosphere to the sea under typical atmospheric conditions (Zhou and Mopper, 1997). In contrast, the carbonyl compounds with three or more carbon atoms and low apparent partition coefficients (lower than 10 M atm^{-1}) are the ones with the lowest solubilities and highest rates of transfer to the gas boundary layer, suggesting that their net flux is likely from the sea to the atmosphere (Zhou and Mopper, 1990b, 1997). Among these, propanal, butanal and octanal showed particularly high transfer rates to overlying atmosphere. Even though the photochemical activity of these compounds did not seem to be influenced by the phytoplankton bloom (see Sect. 3.2), their elevated rates of transfer to the gas phase suggest that the possibility of potential losses to the gas phase during the irradiation experiments should be considered. These compounds have been detected in both the sea surface and the overlying atmosphere (Schlundt et al., 2017), and models propose the Pacific Ocean as a major source of propanal to the atmosphere (Singh et al., 2003).

These results aim to serve as a preliminary basis for motivating new experimental efforts and refining air–sea exchange models, particularly by highlighting the role of the SML in the photochemical production of carbonyl compounds and its implications in the formation of SOAs. We note that these estimations neglect the potential contribution of in situ loss processes within the SML, such as photolysis and microbial consumption, which may substantially decrease the fraction of photochemically-produced carbonyl compounds available for volatilization under ambient conditions. For this reason, the transfer rates presented in the

Table 2. Estimated rates of transfer of photochemically-produced carbonyl compounds from the SML to the gas interface (c_{sl}) according to equilibrium partitioning.

Compound	Apparent partition coefficient ($M\,atm^{-1}$)	Rate of transfer – Non-bloom (molec. $cm^{-2}\,h^{-1}$)	Rate of transfer – Bloom (molec. $cm^{-2}\,h^{-1}$)
Acetophenone	110[a]	2–38 ($\times 10^2$)	2–11 ($\times 10^2$)
Acrolein	7.4[b]	11–5544 ($\times 10^3$)	2–19 ($\times 10^6$)
Benzaldehyde	33.5[c]	9–13 ($\times 10^4$)	Not available
Biacetyl*	65.5[a,b]	16–119 ($\times 10^3$)	12–200 ($\times 10^3$)
Butanal	6.3[c]	3–9 ($\times 10^5$)	5–56 ($\times 10^5$)
Crotonaldehyde	52[d]	10–24 ($\times 10^4$)	2–71 ($\times 10^4$)
Glyoxal	360 000[c]	11–57	4–134
Heptanal	2.0[c]	4–10 ($\times 10^5$)	5–105 ($\times 10^5$)
Hexanal	3.2[c]	6–41 ($\times 10^5$)	Not available
Methacrolein	6.5[e]	8–151 ($\times 10^4$)	2–258 ($\times 10^5$)
Methylglyoxal	32 000[c]	24–289	40–428
MVK	41[e]	7–68 ($\times 10^4$)	8–711 ($\times 10^4$)
Octanal	1.1[c]	2–20 ($\times 10^5$)	3–158 ($\times 10^4$)
Propanal	10[c]	9–15 ($\times 10^5$)	11–382 ($\times 10^5$)
Trans-2-hexenal	20[d]	6–30 ($\times 10^3$)	1–2 ($\times 10^4$)

* Average value; [a] Betterton (1991); [b] Snider and Dawson (1985); [c] Zhou and Mopper (1990b), measured in seawater; [d] Buttery et al. (1971); [e] Iraci et al. (1999).

present study shall be interpreted as upper-limit approximations.

While these transfer estimates based on equilibrium partitioning provide useful upper limits, an air–sea transfer estimate based on concentration gradients was explored for glyoxal as a case study, integrating measured SML concentrations under bloom and non-bloom conditions with representative atmospheric values (Sect. S5.2 in the Supplement). The resulting transfer fluxes range between (1.7–20.8) $\times 10^{-4}$ nmol $cm^{-2}\,s^{-1}$ in non-bloom conditions, and (4.1–29.4) $\times 10^{-4}$ nmol $cm^{-2}\,s^{-1}$. In contrast to the rates of transfer of photochemically-produced carbonyl compounds calculated using equilibrium partitioning (Sect. S5.1 in the Supplement), the transfer fluxes estimated using the concentration gradient approach consider total glyoxal concentrations measured in the non-irradiated SML and in the atmosphere in the marine environment. This means that the gradient-based transfer fluxes reflect overall values that integrate all possible processes, while the results obtained in Sect. S5.1 are limited to the photochemically-produced compounds.

Overall, the increased transfer rates observed for several carbonyl compounds during the phytoplankton bloom highlight the need to incorporate the complex interplay of biotic and abiotic factors into marine VOC inventories, which may help to reduce discrepancies between model predictions and real-world observations, especially in coastal areas where blooms are frequent. Additionally, it is important to note that high production in the SML does not necessarily imply higher atmospheric concentrations. Because fluxes in the air–sea interface can be bidirectional, both emission and deposition processes should be taken into account when assessing the atmospheric significance of the SML photochemistry. Future experimental efforts should aim to quantify the photochemical production and volatilization of these carbonyl compounds simultaneously in both the gas and liquid phase to improve the accuracy of our estimations and evaluate more precisely the atmospheric impact of these processes.

4 Summary and conclusions

The SML is a unique and dynamic environment characterized by its high concentrations of OM and its direct exposure to strong solar radiation, making it a potential hotspot for photochemical reactions. In this study, we have assessed the photochemistry in SML and ULW samples collected in a mesocosm experiment where a phytoplankton bloom was induced by the controlled addition of inorganic nutrients. We explored two complementary aspects: (1) photochemical production of 17 atmospherically-relevant carbonyl compounds, and (2) overall photooxidation capacity of the system.

All the target carbonyl compounds were consistently enriched in the SML compared to ULW, supporting the role of the SML as a distinct habitat for abiotic processes. The concentrations in the SML of acetophenone, acrolein, biacetyl, butanal, crotonaldehyde, glyoxal, heptanal, hexanal, methacrolein, methylglyoxal, MVK, octanal, propanal and trans-2-hexenal were higher during the phytoplankton bloom, which is likely the phase of the higher biologi-

cal productivity and enrichment in reactive organic material. The photochemical activity in the SML of acrolein, biacetyl, butanal, crotonaldehyde, glyoxal, heptanal, hexanal, methacrolein, methylglyoxal, MVK, propanal and trans-2-hexenal (primarily isoprene- and lipid-derived products) was particularly higher under bloom conditions, suggesting a link between photochemical reactivity and bloom-induced OM composition changes. The calculation of AQYs suggests that the SML is a more photochemically efficient environment compared to ULW, particularly in the bloom phase of the study. No systematic relationship was found between AQYs and DOC concentrations, which indicates that OM abundance alone does not control the efficiency of the investigated processes. The photochemical production rates of glyoxal and methylglyoxal calculated in this study are similar to those previously published under comparable conditions.

To complement these findings, we have evaluated the photooxidation capacity of SML and ULW samples in the along the mesocosm experiment via EPR spectroscopy, using a CMH probe to monitor the photochemical production of ROS and redox compounds. The estimated overall photooxidation rates remained similar in the three phases of the bloom, and they were comparable between the SML and ULW samples. After accounting for the differences in DOC levels measured along the mesocosm study, these results indicate that photooxidation capacity cannot be solely explained by variations of OM abundance. Instead, they suggest a dominance of redox-active species, such as metal ions, rather than by biological processes.

Overall, our findings reveal that phytoplankton blooms enhance photochemical production of carbonyl compounds in the SML, but appear to have limited direct impact in the photooxidation capacity of these systems. These results suggest that photochemistry in the SML is governed by the complex interaction between biological activity and chemical composition, including OM and redox-active species such as trace metals. Our work provides a novel perspective on how photochemical processes respond to biological events in the seasurface, and points to them as potential sources of VOCs to the marine atmosphere.

While our observations are based on a single mesocosm study, further field verification of our findings are necessary to explore how broader environmental factors, such us nutrient availability, phytoplankton composition, temperature, wind stress, solar radiation and trace metals, can also influence these processes regionally and globally.

Code availability. No custom software code was developed for this study. Data collection, analysis and visualization was performed using standard functions in OriginPro 2023, Microsoft Excel, Agilent Enhanced MassHunter, Agilent MassHunter Qualitative Analysis 10.0, Agilent MassHunter Quantitative Analysis (for GCMS and LCMS), SpinCount (Bruker Corporation) and SPECTRA 6.2, which are commercially available.

Data availability. The dataset that supports the findings of this study is available in Excel sheet format at the Zenodo data repository and can be accessed via https://doi.org/10.5281/zenodo.18725724 (Jibaja Valderrama, 2026).

Supplement. The supplement related to this article is available online at https://doi.org/10.5194/bg-23-1965-2026-supplement.

Author contributions. The study was conceptualized by OJV, DSF, TS, MvP and HH. OJV and DSF wrote the manuscript with contributions from TS, MvP, KWF and HH. OJV participated in the mesocosm study where the seawater samples were collected. OJV optimized the presented analytical method for carbonyl compound quantification with support from MvP, performed the experiments and treated the data with support from MvP and TS. DSF developed the analytical method for the measurement of the photooxidation capacity, performed the experiments and treated the data. KWF developed the method for the trace metals analysis, performed the experiments and treated the data. All co-authors proofread and commented on the manuscript.

Competing interests. The contact author has declared that none of the authors has any competing interests.

Disclaimer. Publisher's note: Copernicus Publications remains neutral with regard to jurisdictional claims made in the text, published maps, institutional affiliations, or any other geographical representation in this paper. The authors bear the ultimate responsibility for providing appropriate place names. Views expressed in the text are those of the authors and do not necessarily reflect the views of the publisher.

Special issue statement. This article is part of the special issue "Biogeochemical processes and Air–sea exchange in the Sea-Surface microlayer (BG/OS inter-journal SI)". It is not associated with a conference.

Acknowledgements. We thank Sylvia Haferkorn, Frederik Nowak and Elena Poschart for supporting the optimization of the GC-MS method and for fruitful discussions. We also thank Bochao Yang for his support in the measurement of samples using EPR spectroscopy. We thank the ICBM for the possibility to use their infrastructure during the mesocosm study.

Financial support. This research was supported by the project "Biogeochemical processes and Air-sea exchange in the Sea-Surface microlayer (BASS)", which was funded by the Deutsche Forschungsgemeinschaft (DFG, German Research Foundation) (grant nos. 451574234 and HE3086/54-1), and by the project RE-

ACTE, which was funded by the ANR/DFG (grant no. HE3086/55-1).

Review statement. This paper was edited by Peter S. Liss and reviewed by two anonymous referees.

References

Andrews, S. S., Caron, S., and Zafiriou, O. C.: Photochemical oxygen consumption in marine waters: A major sink for colored dissolved organic matter?, Limnol. Oceanogr., 45, 267–277, https://doi.org/10.4319/lo.2000.45.2.0267, 2000.

Arangio, A. M., Tong, H., Socorro, J., Pöschl, U., and Shiraiwa, M.: Quantification of environmentally persistent free radicals and reactive oxygen species in atmospheric aerosol particles, Atmos. Chem. Phys., 16, 13105–13119, https://doi.org/10.5194/acp-16-13105-2016, 2016.

Atkinson, R.: Atmospheric chemistry of VOCs and NO_x, Atmos. Environ., 34, 2063–2101, https://doi.org/10.1016/S1352-2310(99)00460-4, 2000.

Balls, P. W.: Copper, lead and cadmium in coastal waters of the western North-Sea, Mar. Chem., 15, 363–378, https://doi.org/10.1016/0304-4203(85)90047-7, 1985.

Berg, S. M., Whiting, Q. T., Herrli, J. A., Winkels, R., Wammer, K. H., and Remucal, C. K.: The Role of Dissolved Organic Matter Composition in Determining Photochemical Reactivity at the Molecular Level, Environ. Sci. Technol., 53, 11725–11734, https://doi.org/10.1021/acs.est.9b03007, 2019.

Betterton, E. A.: The partitioning of ketones between the gas and aqueous phases, Atmos. Environ. A, Gen. Top., 25, 1473–1477, https://doi.org/10.1016/0960-1686(91)90006-S, 1991.

Bianco, A., Sordello, F., Ehn, M., Vione, D., and Passananti, M.: Degradation of nanoplastics in the environment: Reactivity and impact on atmospheric and surface waters, Sci. Total Environ., 742, https://doi.org/10.1016/j.scitotenv.2020.140413, 2020.

Bibi, R., Ribas-Ribas, M., Jaeger, L., Lehners, C., Gassen, L., Cortés-Espinoza, E. F., Wollschläger, J., Thölen, C., Waska, H., Zöbelein, J., Brinkhoff, T., Athale, I., Röttgers, R., Novak, M., Engel, A., Barthelmeß, T., Karnatz, J., Reinthaler, T., Spriahailo, D., Friedrichs, G., Schäfer, F. A., and Wurl, O.: Biogeochemical dynamics of the sea-surface microlayer in a multidisciplinary mesocosm study, Biogeosciences, 22, 7563–7589, https://doi.org/10.5194/bg-22-7563-2025, 2025.

Boonprab, K., Matsui, K., Yoshida, M., Akakabe, Y., Chirapart, A., and Kajiwara, T.: C6-aldehyde formation by fatty acid hydroperoxide lyase in the brown alga Laminaria angustata, Z. Naturforsch. C, 58, 207–214, https://doi.org/10.1515/znc-2003-3-412, 2003.

Briedé, J. J., De Kok, T. M. C. M., Hogervorst, J. G. F., Moonen, E. J. C., Den Camp, C. L. B. O., and Kleinjans, J. C. S.: Development and application of an electron spin resonance spectrometry method for the determination of oxygen free radical formation by particulate matter, Environ. Sci. Technol., 39, 8420–8426, https://doi.org/10.1021/es0485311, 2005.

Buttery, R. G., Bomben, J. L., Guadagni, D. G., and Ling, L. C.: Volatilities of organic flavor compounds in foods, J. Agr. Food Chem., 19, 1045–1048, https://doi.org/10.1021/jf60178a004, 1971.

Calza, P., Vione, D., and Minero, C.: The role of humic and fulvic acids in the phototransformation of phenolic compounds in seawater, Sci. Total Environ., 493, 411–418, https://doi.org/10.1016/j.scitotenv.2014.05.145, 2014.

Carpenter, L. J. and Nightingale, P. D.: Chemistry and Release of Gases from the Surface Ocean, Chem. Rev., 115, 4015–4034, https://doi.org/10.1021/cr5007123, 2015.

Cho, K., Ueno, M., Liang, Y., Kim, D., and Oda, T.: Generation of Reactive Oxygen Species (ROS) by Harmful Algal Bloom (HAB)-Forming Phytoplankton and Their Potential Impact on Surrounding Living Organisms, Antioxidants, 11, https://doi.org/10.3390/antiox11020206, 2022.

Chu, C. H., Lundeen, R. A., Remucal, C. K., Sander, M., and McNeill, K.: Enhanced Indirect Photochemical Transformation of Histidine and Histamine through Association with Chromophoric Dissolved Organic Matter, Environ. Sci. Technol., 49, 5511–5519, https://doi.org/10.1021/acs.est.5b00466, 2015.

Ciuraru, R., Fine, L., van Pinxteren, M., D'Anna, B., Herrmann, H., and George, C.: Unravelling New Processes at Interfaces: Photochemical Isoprene Production at the Sea Surface, Environ. Sci. Technol., 49, 13199–13205, https://doi.org/10.1021/acs.est.5b02388, 2015.

Coble, P. G.: Marine Optical Biogeochemistry: The Chemistry of Ocean Color, Chem. Rev., 107, 402–418, https://doi.org/10.1021/cr050350+, 2007.

Conte, L., Szopa, S., Aumont, O., Gros, V., and Bopp, L.: Sources and Sinks of Isoprene in the Global Open Ocean: Simulated Patterns and Emissions to the Atmosphere, J. Geophys. Res. Oceans, 125, https://doi.org/10.1029/2019JC015946, 2020.

Dai, Y., Yang, S. B., Zhao, D., Hu, C. M., Xu, W., Anderson, D. M., Li, Y., Song, X. P., Boyce, D. G., Gibson, L., Zheng, C. M., and Feng, L.: Coastal phytoplankton blooms expand and intensify in the 21st century, Nature, 615, 280–284, https://doi.org/10.1038/s41586-023-05760-y, 2023.

Dalrymple, R. M., Carfagno, A. K., and Sharpless, C. M.: Correlations between Dissolved Organic Matter Optical Properties and Quantum Yields of Singlet Oxygen and Hydrogen Peroxide, Environ. Sci. Technol., 44, 5824–5829, https://doi.org/10.1021/es101005u, 2010.

Davidson, M. R., Mitchell, S. A., and Bradley, R. H.: Surface studies of low molecular weight photolysis products from UV-ozone oxidised polystyrene, Surf. Sci., 581, 169–177, https://doi.org/10.1016/j.susc.2005.02.049, 2005.

de Bruyn, W. J., Clark, C. D., Pagel, L., and Takehara, C.: Photochemical production of formaldehyde, acetaldehyde and acetone from chromophoric dissolved organic matter in coastal waters, J. Photoch. Photobio. A, 226, 16–22, https://doi.org/10.1016/j.jphotochem.2011.10.002, 2011.

de Bruyn, W. J., Clark, C. D., Senstad, M., Barashy, O., and Hok, S.: The biological degradation of acetaldehyde in coastal seawater, Mar. Chem., 192, 13–21, https://doi.org/10.1016/j.marchem.2017.02.008, 2017.

Deguillaume, L., Leriche, M., Desboeufs, K., Mailhot, G., George, C., and Chaumerliac, N.: Transition metals in atmospheric liquid phases: Sources, reactivity, and sensitive parameters, Chem. Rev., 105, 3388–3431, https://doi.org/10.1021/cr040649c, 2005.

Dixon, J. L., Beale, R., Sargeant, S. L., Tarran, G. A., and Nightingale, P. D.: Microbial acetone oxidation in coastal seawater, Front. Microbiol., 5, https://doi.org/10.3389/fmicb.2014.00243, 2014.

Duinker, J. C. and Nolting, R. F.: Dissolved copper, zinc and cadmium in the Southern Bight of the North Sea, Mar. Pollut. Bull., 13, 93–96, https://doi.org/10.1016/0025-326x(82)90199-0, 1982.

Ehrhardt, M. and Petrick, G.: On the sensitized photo-oxidation of alkylbenzenes in seawater, Mar. Chem., 15, 47–58, https://doi.org/10.1016/0304-4203(84)90037-9, 1984.

Ehrhardt, M., Bouchertall, F., and Hopf, H. P.: Aromatic ketones concentrated from Baltic Sea water, Mar. Chem., 11, 449–461, https://doi.org/10.1016/0304-4203(82)90010-X, 1982.

Engel, A., Bange, H. W., Cunliffe, M., Burrows, S. M., Friedrichs, G., Galgani, L., Herrmann, H., Hertkorn, N., Johnson, M., Liss, P. S., Quinn, P. K., Schartau, M., Soloviev, A., Stolle, C., Upstill-Goddard, R. C., van Pinxteren, M., and Zäncker, B.: The Ocean's Vital Skin: Toward an Integrated Understanding of the Sea Surface Microlayer, Front. Mar. Sci., 4, https://doi.org/10.3389/fmars.2017.00165, 2017.

Epstein, S. A., Tapavicza, E., Furche, F., and Nizkorodov, S. A.: Direct photolysis of carbonyl compounds dissolved in cloud and fog droplets, Atmos. Chem. Phys., 13, 9461–9477, https://doi.org/10.5194/acp-13-9461-2013, 2013.

Fabbri, D., Carena, L., Bertone, D., Brigante, M., Passananti, M., and Vione, D.: Assessing the photodegradation potential of compounds derived from the photoinduced weathering of polystyrene in water, Sci. Total Environ., 876, https://doi.org/10.1016/j.scitotenv.2023.162729, 2023.

Ferrario, J. B., Lawler, G. C., Deleon, I. R., and Laseter, J. L.: Volatile Organic Pollutants in Biota and Sediments of Lake Pontchartrain, Bull. Environ. Contam. Toxicol., 34, 246–255, https://doi.org/10.1007/BF01609730, 1985.

Fomba, K. W., Müller, K., van Pinxteren, D., and Herrmann, H.: Aerosol size-resolved trace metal composition in remote northern tropical Atlantic marine environment: case study Cape Verde islands, Atmos. Chem. Phys., 13, 4801–4814, https://doi.org/10.5194/acp-13-4801-2013, 2013.

Fomba, K. W., Deabji, N., Barcha, S. E. I., Ouchen, I., Elbaramoussi, E. M., El Moursli, R. C., Harnafi, M., El Hajjaji, S., Mellouki, A., and Herrmann, H.: Application of TXRF in monitoring trace metals in particulate matter and cloud water, Atmos. Meas. Tech., 13, 4773–4790, https://doi.org/10.5194/amt-13-4773-2020, 2020.

Fu, T. M., Jacob, D. J., Wittrock, F., Burrows, J. P., Vrekoussis, M., and Henze, D. K.: Global budgets of atmospheric glyoxal and methylglyoxal, and implications for formation of secondary organic aerosols, J. Geophys. Res. Atmos., 113, https://doi.org/10.1029/2007jd009505, 2008.

Fujii, M. and Otani, E.: Photochemical generation and decay kinetics of superoxide and hydrogen peroxide in the presence of standard humic and fulvic acids, Water Res., 123, 642–654, https://doi.org/10.1016/j.watres.2017.07.015, 2017.

González-Davila, M., Santana-Casiano, J. M., and Millero, F. J.: Oxidation of iron (II) nanomolar with H_2O_2 in seawater, Geochim. Cosmochim. Acta, 68, 83–93, https://doi.org/10.1016/j.gca.2004.05.043, 2004.

Gotham, J. P., Li, R., Tipple, T. E., Lancaster, J. R., Liu, T. M., and Li, Q.: Quantitation of spin probe-detectable oxidants in cells using electron paramagnetic resonance spectroscopy: To probe or to trap?, Free Radic. Bio. Med., 154, 84–94, https://doi.org/10.1016/j.freeradbiomed.2020.04.020, 2020.

Grandbois, M., Latch, D. E., and Mcneill, K.: Microheterogeneous Concentrations of Singlet Oxygen in Natural Organic Matter Isolate Solutions, Environ. Sci. Technol., 42, 9184–9190, https://doi.org/10.1021/es8017094, 2008.

Hansard, S. P., Vermilyea, A. W., and Voelker, B. M.: Measurements of superoxide radical concentration and decay kinetics in the Gulf of Alaska, Deep-Sea Res. I, 57, 1111–1119, https://doi.org/10.1016/j.dsr.2010.05.007, 2010.

Hansel, C. M. and Diaz, J. M.: Production of Extracellular Reactive Oxygen Species by Marine Biota, Annu. Rev. Mar. Sci., 13, 177–200, https://doi.org/10.1146/annurev-marine-041320-102550, 2021.

Hansell, D. A. and Carlson, C. A.: Biogeochemistry of Marine Dissolved Organic Matter, Academic Press, London, ISBN 978-0-443-13858-4, 2002.

Hardy, J. T.: The sea-surface microlayer: Biology, chemistry and anthropogenic enrichment, Prog. Oceanogr., 11, 307–328, https://doi.org/10.1016/0079-6611(82)90001-5, 1982.

Harvey, G. W. and Burzell, L. A.: Simple Microlayer Method for Small Samples, Limnol. Oceanogr., 17, 156–157, https://doi.org/10.4319/lo.1972.17.1.0156, 1972.

Hatchard, C. G. and Parker, C. A.: A New Sensitive Chemical Actinometer. I I. Potassium Ferrioxalate as a Standard Chemical Actinometer, Proc. R. Soc. Lon. A Math. Phys. Sci., 235, 518–536, https://doi.org/10.1098/rspa.1956.0102, 1956.

Huang, D., Zhang, X., Chen, Z. M., Zhao, Y., and Shen, X. L.: The kinetics and mechanism of an aqueous phase isoprene reaction with hydroxyl radical, Atmos. Chem. Phys., 11, 7399–7415, https://doi.org/10.5194/acp-11-7399-2011, 2011.

Iraci, L. T., Baker, B. M., Tyndall, G. S., and Orlando, J. J.: Measurements of the Henry's law coefficients of 2-Methyl-3-buten-2-ol, Methacrolein, and Methylvinyl ketone, J. Atmos. Chem., 33, 321–330, https://doi.org/10.1023/A:1006169029230, 1999.

Jaoui, M., Nestorowicz, K., Rudzinski, K. J., Lewandowski, M., Kleindienst, T. E., Torres, J., Bulska, E., Danikiewicz, W., and Szmigielski, R.: Atmospheric oxidation of 1,3-butadiene: influence of seed aerosol acidity and relative humidity on SOA composition and the production of air toxic compounds, Atmos. Chem. Phys., 25, 1401–1432, https://doi.org/10.5194/acp-25-1401-2025, 2025.

Jibaja Valderrama, O.: Photochemistry of the sea-surface microlayer (SML) influenced by a phytoplankton bloom: a mesocosm study, Zenodo [data set], https://doi.org/10.5281/zenodo.18725724, 2026.

Jiménez, E., Lanza, B., Martínez, E., and Albaladejo, J.: Daytime tropospheric loss of hexanal and *trans*-2-hexenal: OH kinetics and UV photolysis, Atmos. Chem. Phys., 7, 1565–1574, https://doi.org/10.5194/acp-7-1565-2007, 2007.

Jomova, K. and Valko, M.: Advances in metal-induced oxidative stress and human disease, Toxicology, 283, 65–87, https://doi.org/10.1016/j.tox.2011.03.001, 2011.

Kato, S., Shimizu, N., Otoki, Y., Ito, J., Sakaino, M., Sano, T., Takeuchi, S., Imagi, J., and Nakagawa, K.: Determination of acrolein generation pathways from linoleic acid and linolenic

acid: increment by photo irradiation, Npj Sci. Food, 6, https://doi.org/10.1038/s41538-022-00138-2, 2022.

Kieber, R. J., Zhou, X. L., and Mopper, K.: Formation of carbonyl compounds from UV-Induced photodegradation of humic substances in natural waters: Fate of riverine carbon in the sea, Limnol. Oceanogr., 35, 1503–1515, https://doi.org/10.4319/lo.1990.35.7.1503, 1990.

Kuhn, H. J., Braslavsky, S. E., and Schmidt, R.: Chemical actinometry, Pure Appl. Chem., 76, 2105–2146, https://doi.org/10.1351/pac200476122105, 2004.

Lampert, W.: Release of dissolved organic carbon by grazing zooplankton, Limnol. Oceanogr., 23, 831–834, https://doi.org/10.4319/lo.1978.23.4.0831, 1978.

Lancelot, C.: Gross excretion rates of natural marine phytoplankton and heterotrophic uptake of excreted products in the southern North Sea, as determined by short-term kinetics, Mar. Ecol. Prog. Ser., 1, 179–186, https://doi.org/10.3354/meps001179, 1979.

Liss, P. S. and Slater, P. G.: Flux of Gases Across Air–Sea Interface, Nature, 247, 181–184, https://doi.org/10.1038/247181a0, 1974.

Liss, P. S., Watson, A. J., Bock, E. J., Jahne, B., Asher, W. E., Frew, N. M., Hasse, L., Korenowski, G. M., Merlivat, L., Phillips, L. F., Schluessel, P., and Woolf, D. K.: The Sea Surface and Global Change, Cambridge University Press, Cambridge, ISBN 978-0-521-56273-2, 1997.

Lueder, U., Jorgensen, B. B., Kappler, A., and Schmidt, C.: Photochemistry of iron in aquatic environments, Environ. Sci.: Process. Impacts, 22, 12–24, https://doi.org/10.1039/c9em00415g, 2020.

Mart, L. and Nurnberg, H. W.: Cd, Pb, Cu, Ni and Co distribution in the German Bight, Mar. Chem., 18, 197–213, https://doi.org/10.1016/0304-4203(86)90008-3, 1986.

McNeill, K. and Canonica, S.: Triplet state dissolved organic matter in aquatic photochemistry: reaction mechanisms, substrate scope, and photophysical properties, Environ. Sci. Process. Impacts, 18, 1381–1399, https://doi.org/10.1039/c6em00408c, 2016.

Millero, F. J.: Solubility of Fe(III) in seawater, Earth Planet. Sc. Lett., 154, 323–329, https://doi.org/10.1016/S0012-821x(97)00179-9, 1998.

Millero, F. J., Sotolongo, S., and Izaguirre, M.: The oxidation kinetics of Fe(II) in seawater, Geochim. Cosmochim. Acta, 51, 793–801, https://doi.org/10.1016/0016-7037(87)90093-7, 1987.

Millero, F. J., Sharma, V. K., and Karn, B.: The rate of reduction of copper(II) with hydrogen peroxide in seawater, Mar. Chem., 36, 71–83, https://doi.org/10.1016/S0304-4203(09)90055-X, 1991.

Millet, D. B., Guenther, A., Siegel, D. A., Nelson, N. B., Singh, H. B., de Gouw, J. A., Warneke, C., Williams, J., Eerdekens, G., Sinha, V., Karl, T., Flocke, F., Apel, E., Riemer, D. D., Palmer, P. I., and Barkley, M.: Global atmospheric budget of acetaldehyde: 3-D model analysis and constraints from in-situ and satellite observations, Atmos. Chem. Phys., 10, 3405–3425, https://doi.org/10.5194/acp-10-3405-2010, 2010.

Milne, P. J., Riemer, D. D., Zika, R. G., and Brand, L. E.: Measurement of vertical distribution of isoprene in surface seawater, Its chemical fate, and its emission from several phytoplankton monocultures, Mar. Chem., 48, 237–244, https://doi.org/10.1016/0304-4203(94)00059-M, 1995.

Moan, J., Hovik, B., and Wold, E.: Two New Methods of Actinometry for EPR-Measurements, Photochem. Photobiol., 30, 623–624, https://doi.org/10.1111/j.1751-1097.1979.tb07189.x, 1979.

Moffett, J. W. and Zika, R. G.: Oxidation kinetics of Cu(I) in seawater: implications for its existence in the marine environment, Mar. Chem., 13, 239–251, https://doi.org/10.1016/0304-4203(83)90017-8, 1983.

Moffett, J. W. and Zika, R. G.: Reaction kinetics of hydrogen peroxide with copper and iron in seawater, Environ. Sci. Technol., 21, 804–810, https://doi.org/10.1021/es00162a012, 1987.

Momzikoff, A., Santus, R., and Giraud, M.: A study of the photosensitizing properties of seawater, Mar. Chem., 12, 1–14, https://doi.org/10.1016/0304-4203(83)90024-5, 1983.

Moore, R. M., Oram, D. E., and Penkett, S. A.: Production of isoprene by marine phytoplankton cultures, Geophys. Res. Lett., 21, 2507–2510, https://doi.org/10.1029/94GL02363, 1994.

Mopper, K. and Stahovec, W. L.: Sources and sinks of low molecular weight organic carbonyl compounds in seawater, Mar. Chem., 19, 305–321, https://doi.org/10.1016/0304-4203(86)90052-6, 1986.

Mopper, K. and Zhou, X. L.: Hydroxyl Radical Photoproduction in the Sea and Its Potential Impact on Marine Processes, Science, 250, 661–664, https://doi.org/10.1126/science.250.4981.661, 1990.

Mopper, K., Zhou, X. L., Kieber, R. J., Kieber, D. J., Sikorski, R. J., and Jones, R. D.: Photochemical degradation of dissolved organic carbon and its impact on the oceanic carbon cycle, Nature, 353, 60–62, https://doi.org/10.1038/353060a0, 1991.

Nishimura, T., Hara, K., Honda, N., Okazaki, S., Hazama, H., and Awazu, K.: Determination and analysis of singlet oxygen quantum yields of talaporfin sodium, protoporphyrin IX, and lipidated protoporphyrin IX using near-infrared luminescence spectroscopy, Lasers Med. Sci., 35, 1289–1297, https://doi.org/10.1007/s10103-019-02907-0, 2020.

Nolting, R. F.: Copper, zinc, cadmium, nickel, iron and manganese in the Southern Bight of the North Sea, Mar. Pollut. Bull., 17, 113–117, https://doi.org/10.1016/0025-326X(86)90415-7, 1986.

Onyango, A. N.: Small reactive carbonyl compounds as tissue lipid oxidation products; and the mechanisms of their formation thereby, Chem. Phys. Lipids, 165, 777–786, https://doi.org/10.1016/j.chemphyslip.2012.09.004, 2012.

Penezic, A., Wang, X. K., Perrier, S., George, C., and Frka, S.: Interfacial photochemistry of marine diatom lipids: Abiotic production of volatile organic compounds and new particle formation, Chemosphere, 313, https://doi.org/10.1016/j.chemosphere.2022.137510, 2023.

Rabani, J., Mamane, H., Pousty, D., and Bolton, J. R.: Practical Chemical Actinometry – A Review, Photochem. Photobiol., 97, 873–902, https://doi.org/10.1111/php.13429, 2021.

Rocco, M., Dunne, E., Peltola, M., Barr, N., Williams, J., Colomb, A., Safi, K., Saint-Macary, A., Marriner, A., Deppeler, S., Harnwell, J., Law, C., and Sellegri, K.: Oceanic phytoplankton are a potentially important source of benzenoids to the remote marine atmosphere, Commun. Earth Environ., 2, https://doi.org/10.1038/s43247-021-00253-0, 2021.

Rochelle-Newall, E. J., Fisher, T. R., Fan, C., and Glibert, P. M.: Dynamics of chromophoric dissolved organic matter and dissolved organic carbon in experimental mesocosms, Int. J. Remote Sens., 20, 627–641, https://doi.org/10.1080/014311699213389, 1999.

Rodigast, M., Mutzel, A., Iinuma, Y., Haferkorn, S., and Herrmann, H.: Characterisation and optimisation of a sample preparation method for the detection and quantification of atmospherically relevant carbonyl compounds in aqueous medium, Atmos. Meas. Tech., 8, 2409–2416, https://doi.org/10.5194/amt-8-2409-2015, 2015.

Sander, R.: Compilation of Henry's law constants (version 5.0.0) for water as solvent, Atmos. Chem. Phys., 23, 10901–12440, https://doi.org/10.5194/acp-23-10901-2023, 2023.

Scheres Firak, D., Schaefer, T., Yang, B., Jibaja Valderrama, O., van Pinxteren, M., and Herrmann, H.: Coupling Aqueous Phase Chemical Actinometry with EPR Spectroscopy: An Approach for Probing Photochemical Processes at the Air–Sea Interface, ChemPhysChem., 27, e202500734, https://doi.org/10.1002/cphc.202500734, 2026.

Schlundt, C., Tegtmeier, S., Lennartz, S. T., Bracher, A., Cheah, W., Krüger, K., Quack, B., and Marandino, C. A.: Oxygenated volatile organic carbon in the western Pacific convective center: ocean cycling, air–sea gas exchange and atmospheric transport, Atmos. Chem. Phys., 17, 10837–10854, https://doi.org/10.5194/acp-17-10837-2017, 2017.

Schobert, B. and Elstner, E. F.: Production of Hexanal and Ethane by Phaeodactylum-Triconutum and Its Correlation to Fatty Acid Oxidation and Bleaching of Photosynthetic Pigments, Plant Physiol., 66, 215–219, https://doi.org/10.1104/pp.66.2.215, 1980.

Scully, N. M., McQueen, D. J., Lean, D. R. S., and Cooper, W. J.: Hydrogen peroxide formation: The interaction of ultraviolet radiation and dissolved organic carbon in lake waters along a 43–75° N gradient, Limnol. Oceanogr., 41, 540–548, https://doi.org/10.4319/lo.1996.41.3.0540, 1996.

Sharma, V. K. and Millero, F. J.: Oxidation of copper(I) in seawater, Environ. Sci. Technol., 22, 768–771, https://doi.org/10.1021/es00172a004, 1988.

Shaw, S. L., Chisholm, S. W., and Prinn, R. G.: Isoprene production by Prochlorococcus, a marine cyanobacterium, and other phytoplankton, Mar. Chem., 80, 227–245, https://doi.org/10.1016/S0304-4203(02)00101-9, 2003.

Siems, A., Zimmermann, T., Sanders, T., and Pröfrock, D.: Dissolved trace elements and nutrients in the North Sea – A current baseline, Environ. Monit. Assess., 196, https://doi.org/10.1007/s10661-024-12675-2, 2024.

Simó, R., Cortés-Greus, P., Rodríguez-Ros, P., and Masdeu-Navarro, M.: Substantial loss of isoprene in the surface ocean due to chemical and biological consumption, Commun. Earth Environ., 3, https://doi.org/10.1038/s43247-022-00352-6, 2022.

Singh, H. B., Tabazadeh, A., Evans, M. J., Field, B. D., Jacob, D. J., Sachse, G., Crawford, J. H., Shetter, R., and Brune, W. H.: Oxygenated volatile organic chemicals in the oceans: Inferences and implications based on atmospheric observations and air–sea exchange models, Geophys. Res. Lett., 30, https://doi.org/10.1029/2003gl017933, 2003.

Sinha, V., Williams, J., Meyerhöfer, M., Riebesell, U., Paulino, A. I., and Larsen, A.: Air-sea fluxes of methanol, acetone, acetaldehyde, isoprene and DMS from a Norwegian fjord following a phytoplankton bloom in a mesocosm experiment, Atmos. Chem. Phys., 7, 739–755, https://doi.org/10.5194/acp-7-739-2007, 2007.

Snider, J. R. and Dawson, G. A.: Tropospheric light alcohols, carbonyls, and acetonitrile: Concentrations in southwestern United States and Henry's Law data, J. Geophys. Res. Atmos., 90, 3797–3805, https://doi.org/10.1029/JD090iD02p03797, 1985.

Sun, L. H., Wu, C. H., and Faust, B. C.: Photochemical redox reactions of inner-sphere copper(II)-dicarboxylate complexes: Effects of the dicarboxylate ligand structure on copper(I) quantum yields, J. Phys. Chem. A, 102, 8664–8672, https://doi.org/10.1021/jp982045g, 1998.

Sun, L. N., Qian, J. G., Blough, N. V., and Mopper, K.: Insights into the Photoproduction Sites of Hydroxyl Radicals by Dissolved Organic Matter in Natural Waters, Environ, Sci. Technol. Lett., 2, 352–356, https://doi.org/10.1021/acs.estlett.5b00294, 2015.

Tadic, J., Juranic, I., and Moortgat, G. K.: Photooxidation of n-Hexanal in Air, Molecules, 6, 287–299, https://doi.org/10.3390/60400287, 2001.

Thölen, C., Wollschläger, J., Novak, M. G., Röttgers, R., and Zielinski, O.: Colored and Fluorescent DOM in the Sea-Surface Microlayer: Response to a Phytoplankton Bloom and Photodegradation in a Mesocosm Study, EGUsphere [preprint], https://doi.org/10.5194/egusphere-2025-5350, 2026.

Thomalla, S. J., Nicholson, S. A., Ryan-Keogh, T. J., and Smith, M. E.: Widespread changes in Southern Ocean phytoplankton blooms linked to climate drivers, Nat. Clim. Change, 13, 975–984, https://doi.org/10.1038/s41558-023-01768-4, 2023.

Tilgner, A. and Herrmann, H.: Radical-driven carbonyl-to-acid conversion and acid degradation in tropospheric aqueous systems studied by CAPRAM, Atmos. Environ., 44, 5415–5422, https://doi.org/10.1016/j.atmosenv.2010.07.050, 2010.

Tinel, L., Abbatt, J., Saltzman, E., Engel, A., Fernandez, R., Li, Q. Y., Mahajan, A. S., Nicewonger, M., Novak, G., Saiz-Lopez, A., Schneider, S., and Wang, S. S.: Impacts of ocean biogeochemistry on atmospheric chemistry, Elem. Sci. Anth., 11, https://doi.org/10.1525/elementa.2023.00032, 2023.

Tuazon, E. C., Macleod, H., Atkinson, R., and Carter, W. P. L.: Alpha-Dicarbonyl Yields from the NO_x–Air Photooxidations of a Series of Aromatic-Hydrocarbons in Air, Environ. Sci. Technol., 20, 383–387, https://doi.org/10.1021/es00146a010, 1986.

Tuazon, E. C., Alvarado, A., Aschmann, S. M., Atkinson, R., and Arey, J.: Products of the Gas-Phase Reactions of 1,3-Butadiene with OH and NO_3 Radicals, Environ. Sci. Technol., 33, 3586–3595, https://doi.org/10.1021/es990193u, 1999.

Uchida, K., Kanematsu, M., Morimitsu, Y., Osawa, T., Noguchi, N., and Niki, E.: Acrolein Is a Product of Lipid Peroxidation Reaction: Formation of Free Acrolein and Its Conjugate with Lysine Residues in Oxidized Low Density Lipoproteins, J. Biol. Chem., 273, 16058–16066, https://doi.org/10.1074/jbc.273.26.16058, 1998.

van Pinxteren, M. and Herrmann, H.: Glyoxal and methylglyoxal in Atlantic seawater and marine aerosol particles: method development and first application during the Polarstern cruise ANT XXVII/4, Atmos. Chem. Phys., 13, 11791–11802, https://doi.org/10.5194/acp-13-11791-2013, 2013.

Vaughan, P. P. and Blough, N. V.: Photochemical Formation of Hydroxyl Radical by Constituents of Natural Waters, Environ. Sci. Technol., 32, 2947–2953, https://doi.org/10.1021/es9710417, 1998.

Volkamer, R., Platt, U., and Wirtz, K.: Primary and Secondary Glyoxal Formation from Aromatics: Experimental Evidence for the Bicycloalkyl-Radical Pathway from Benzene, Toluene, and *p*-Xylene, J. Phys. Chem. A, 105, 7865–7874, https://doi.org/10.1021/jp010152w, 2001.

Waggoner, D. C., Wozniak, A. S., Cory, R. M., and Hatcher, P. G.: The role of reactive oxygen species in the degradation of lignin derived dissolved organic matter, Geochim. Cosmochim. Acta, 208, 171–184, https://doi.org/10.1016/j.gca.2017.03.036, 2017.

Wagner, S., Schubotz, F., Kaiser, K., Hallmann, C., Waska, H., Rossel, P. E., Hansmann, R., Elvert, M., Middelburg, J. J., Engel, A., Blattmann, T. M., Catalá, T. S., Lennartz, S. T., Gomez-Saez, G. V., Pantoja-Gutiérrez, S., Bao, R., and Galy, V.: Soothsaying DOM: A Current Perspective on the Future of Oceanic Dissolved Organic Carbon, Front. Mar. Sci., 7, https://doi.org/10.3389/fmars.2020.00341, 2020.

Walker, H., Stone, D., Ingham, T., Hackenberg, S., Cryer, D., Punjabi, S., Read, K., Lee, J., Whalley, L., Spracklen, D. V., Carpenter, L. J., Arnold, S. R., and Heard, D. E.: Observations and modelling of glyoxal in the tropical Atlantic marine boundary layer, Atmos. Chem. Phys., 22, 5535–5557, https://doi.org/10.5194/acp-22-5535-2022, 2022.

Wang, S. Y., Hornbrook, R. S., Hills, A., Emmons, L. K., Tilmes, S., Lamarque, J. F., Jimenez, J. L., Campuzano-Jost, P., Nault, E. A., Crounse, J. D., Wennberg, P. O., Kim, M., Allen, H., Ryerson, T. B., Thompson, C. R., Peischl, J., Moore, F., Nance, D., Hall, B., Elkins, J., Tanner, D., Huey, L. G., Hall, S. R., Ullmann, K., Orlando, J. J., Tyndall, G. S., Flocke, F. M., Ray, E., Hanisco, T. F., Wolfe, G. M., St Clair, J., Commane, R., Daube, B., Barletta, B., Blake, D. R., Weinzierl, B., Dollner, M., Conley, A., Vitt, F., Wofsy, S. C., Riemer, D. D., and Apel, E. C.: Atmospheric Acetaldehyde: Importance of Air–Sea Exchange and a Missing Source in the Remote Troposphere, Geophys. Res. Lett., 46, 5601–5613, https://doi.org/10.1029/2019gl082034, 2019.

Wang, Y. Q., Zeng, J. Q., Wu, B. J., Song, W., Hu, W. W., Liu, J. P., Yang, Y., Yu, Z. Q., Wang, X. M., and Gligorovski, S.: Production of Volatile Organic Compounds by Ozone Oxidation Chemistry at the South China Sea Surface Microlayer, ACS Earth Space Chem., 7, 1306–1313, https://doi.org/10.1021/acsearthspacechem.3c00102, 2023.

Williams, R. T., Caspers-Brown, A., Michaud, J., Stevens, N., Meehan, M., Sultana, C. M., Lee, C. S. P., Malfatti, F., Zhou, Y. Y., Azam, F., Prather, K. A., Dorrestein, P., Burkart, M. D., and Pomeroy, R. S.: Possible Missing Sources of Atmospheric Glyoxal Part II: Oxidation of Toluene Derived from the Primary Production of Marine Microorganisms, Metabolites, 14, https://doi.org/10.3390/metabo14110631, 2024.

Wu, H. Y. and Lin, J. K.: Determination of Aldehydic Lipid Peroxidation Products with Dabsylhydrazine by High-Performance Liquid Chromatography, Anal. Chem., 67, 1603–1612, https://doi.org/10.1021/ac00105a020, 1995.

Wurl, O., Wurl, E., Miller, L., Johnson, K., and Vagle, S.: Formation and global distribution of sea-surface microlayers, Biogeosciences, 8, 121–135, https://doi.org/10.5194/bg-8-121-2011, 2011.

Wurl, O., Stolle, C., Van Thuoc, C., Thu, P. T., and Mari, X.: Biofilm-like properties of the sea surface and predicted effects on air–sea CO_2 exchange, Prog. Oceanogr., 144, 15–24, https://doi.org/10.1016/j.pocean.2016.03.002, 2016.

Wurl, O., Ekau, W., Landing, W. M., and Zappa, C. J.: Sea-surface microlayer in a changing ocean – A perspective, Elem. Sci. Anth., 5, https://doi.org/10.1525/elementa.228, 2017.

Yang, L., Zhang, J., Engel, A., and Yang, G.-P.: Spatio-temporal distribution, photoreactivity and environmental control of dissolved organic matter in the sea-surface microlayer of the eastern marginal seas of China, Biogeosciences, 19, 5251–5268, https://doi.org/10.5194/bg-19-5251-2022, 2022.

Zafiriou, O. C.: Marine organic photochemistry previewed, Mar. Chem., 5, 497–522, https://doi.org/10.1016/0304-4203(77)90037-8, 1977.

Zhang, Y., Del Vecchio, R., and Blough, N. V.: Investigating the Mechanism of Hydrogen Peroxide Photoproduction by Humic Substances, Environ. Sci. Technol., 46, 11836–11843, https://doi.org/10.1021/es3029582, 2012.

Zhou, S., Gonzalez, L., Leithead, A., Finewax, Z., Thalman, R., Vlasenko, A., Vagle, S., Miller, L. A., Li, S.-M., Bureekul, S., Furutani, H., Uematsu, M., Volkamer, R., and Abbatt, J.: Formation of gas-phase carbonyls from heterogeneous oxidation of polyunsaturated fatty acids at the air–water interface and of the sea surface microlayer, Atmos. Chem. Phys., 14, 1371–1384, https://doi.org/10.5194/acp-14-1371-2014, 2014.

Zhou, X. L. and Mopper, K.: Determination of photochemically produced hydroxyl radicals in seawater and Freshwater, Mar. Chem., 30, 71–88, https://doi.org/10.1016/0304-4203(90)90062-H, 1990a.

Zhou, X. L. and Mopper, K.: Apparent Partition-Coefficients of 15 Carbonyl Compounds between Air and Seawater and between Air and Freshwater; Implications for Air Sea Exchange, Environ. Sci. Technol., 24, 1864–1869, https://doi.org/10.1021/es00082a013, 1990b.

Zhou, X. L. and Mopper, K.: Photochemical production of low-molecular-weight carbonyl compounds in seawater and surface microlayer and their air–sea exchange, Mar. Chem., 56, 201–213, https://doi.org/10.1016/S0304-4203(96)00076-X, 1997.

Zhu, Y. T. and Kieber, D. J.: Wavelength- and Temperature-Dependent Apparent Quantum Yields for Photochemical Production of Carbonyl Compounds in the North Pacific Ocean, Environ. Sci. Technol., 52, 1929–1939, https://doi.org/10.1021/acs.est.7b05462, 2018.

Zhu, Y. T. and Kieber, D. J.: Concentrations and Photochemistry of Acetaldehyde, Glyoxal, and Methylglyoxal in the Northwest Atlantic Ocean, Environ. Sci. Technol., 53, 9512–9521, https://doi.org/10.1021/acs.est.9b01631, 2019.

Zöbelein, J., Sawle, S., Friedrichs, G., Ribas-Ribas, M., Lehners, C., Paetz, K., Pflaum, M., and Waska, H.: Buoyancy and polarity driven accumulation of dissolved organic matter in the sea surface microlayer during a phytoplankton bloom, EGUsphere [preprint], https://doi.org/10.5194/egusphere-2025-6563, 2026.